Dendritic cell and antigen dispersal landscapes regulate T cell immunity

Michael Y. Gerner,[1] Kerry A. Casey,[2] Wolfgang Kastenmuller,[3] and Ronald N. Germain[4]

[1]Department of Immunology, University of Washington, Seattle, WA
[2]Department of Respiratory, Inflammation and Autoimmunity, MedImmune, LLC, Gaithersburg, MD
[3]Institute of Experimental Immunology, University of Bonn, Bonn, Germany
[4]Lymphocyte Biology Section, Laboratory of Systems Biology, National Institute of Allergy and Infectious Diseases, National Institutes of Health, Bethesda, MD

Dendritic cell (DC) subsets with biased capacity for CD4$^+$ and CD8$^+$ T cell activation are asymmetrically distributed in lymph nodes (LNs), but how this affects adaptive responses has not been extensively studied. Here we used quantitative imaging to examine the relationships among antigen dispersal, DC positioning, and T cell activation after protein immunization. Antigens rapidly drained into LNs and formed gradients extending from the lymphatic sinuses, with reduced abundance in the deep LN paracortex. Differential localization of DCs specialized for major histocompatibility complex I (MHC I) and MHC II presentation resulted in preferential activation of CD8$^+$ and CD4$^+$ T cells within distinct LN regions. Because MHC I–specialized DCs are positioned in regions with limited antigen delivery, modest reductions in antigen dose led to a substantially greater decline in CD8$^+$ compared with CD4$^+$ T cell activation, expansion, and clonal diversity. Thus, the collective action of antigen dispersal and DC positioning regulates the extent and quality of T cell immunity, with important implications for vaccine design.

INTRODUCTION

DCs are the primary antigen-presenting cells that induce activation and differentiation of T lymphocytes in secondary lymphoid tissues, serving as key initiators of adaptive immunity (Merad et al., 2013; Murphy et al., 2016). DCs are subdivided into multiple subsets, as defined by tissue of residence, phenotypic profile, and divergent functional properties with respect to T cell activation. One of the better-characterized dichotomies is the capacity of murine lymphoid tissue resident (CD11c^{HI}MHC-II^{INT}) CD8a$^+$XCR1$^+$CD205$^+$ DCs (also known as cDC1 cells) to mediate MHC I antigen cross-presentation versus the specialization of SIRPa$^+$CD11b$^+$ DCs (also known as cDC2 cells) for MHC II antigen display (Dudziak et al., 2007; Merad et al., 2013; Guilliams et al., 2014; Murphy et al., 2016).

Intriguingly, several studies have demonstrated asymmetric positioning of these DC subsets in the spleen, with the localization of cDC2s within the bridging channels connecting the red and the white pulp, and with the positioning of cDC1s deeper within the T cell zone, although some red pulp cDC1s have also been noted (Steinman et al., 1997; Calabro et al., 2016). Understanding analogous processes in LNs has been more challenging because of the presence of a larger number of DC populations with highly overlapping phenotypic profiles, derived from both LN-resident and peripheral tissue sources. To address this, we have recently developed an analytical microscopy pipeline, histo-cytometry, which permits multiplex phenotypic analysis of cells directly in tissue sections, akin to in situ flow cytometry (Gerner et al., 2012). Using this technique, we demonstrated that major LN-resident and migratory DC populations show preferential residence in distinct regions of steady-state LNs, and in particular that LN-resident cDC1 and cDC2 populations are largely segregated between the deeper paracortical (T cell zone) and lymphatic sinus (LS)–proximal regions, respectively (Gerner et al., 2012). These studies collectively indicate that all secondary lymphoid organs are highly compartmentalized, with individual zones containing unique sets of DC populations.

What does such spatial segregation mean with respect to the generation of innate and adaptive immune responses? Positioning of cDC2s within the bridging channels of the spleen can support their homeostasis through interactions with lymphotoxin-α1/β2–expressing B cells (Gatto et al., 2013; Yi and Cyster, 2013). Importantly, such localization promotes capture of circulating particulate antigens, especially those associated with cells, that are too large to access the T cell zone and leads to efficient induction of CD4$^+$ T cell responses and humoral immunity (Gatto et al., 2013; Yi and Cyster, 2013; Calabro et al., 2016). In a similar fashion, localization of LN-resident cDC2s in close association with the LS in LNs promotes sampling of lymph-borne antigens directly from within the LS lumen and is critical for inducing rapid CD4$^+$ T cell responses to large particulate antigens after immunization or infection of peripheral tissue sites (Gonzalez et al., 2010; Woodruff et al., 2014; Gerner et al., 2015).

Correspondence to Michael Y. Gerner: gernermy@uw.edu

Abbreviations used: APC, allophycocyanin; GP, glycoprotein; HEV, high endothelial venule; LS, lymphatic sinus; pMHC, peptide–MHC.

The Rockefeller University Press
J. Exp. Med. 2017 Vol. 214 No. 10 3105–3122
https://doi.org/10.1084/jem.20170335

In contrast, induction of $CD8^+$ T cell responses appears to be predominantly mediated by cDC1s located deeper within the LN paracortex. Minimal penetration of these regions by large particulate antigens after immunization prohibits efficient uptake by cDC1s and can limit $CD8^+$ T cell activation (Gerner et al., 2015). Even during viral infections, in which $CD8^+$ T cell priming can be initiated by directly infected nonprofessional antigen presenting cells in the LN periphery, generation of functional $CD8^+$ T cell memory still requires priming by the centrally localized LN-resident cDC1s (Eickhoff et al., 2015).

Although there is limited delivery of large particulate antigens to cDC1s positioned in the deep LN paracortex, other antigen types may be more efficient at targeting this region. In this regard, smaller (<70 kD) proteins, dextrans, immunomodulatory cytokines, and chemokines are able to rapidly enter the LN conduit system, which connects the LS with the high endothelial venules (HEVs) and the T cell zone (Lämmermann and Sixt, 2008; Roozendaal et al., 2008; Rantakari et al., 2015). Further, LN-resident DCs have been suggested to place dendritic processes inside the conduit lumen and capture antigens for presentation to T cells (Sixt et al., 2005), indicating that delivery of small protein antigens via the conduit network may result in improved $CD8a^+$ DC targeting. However, conduits are not uniformly distributed throughout the LN, with a sparser composition in the deep T cell zone (Katakai et al., 2004). Ultrastructural studies also indicate presence of thick collagen fibers within the conduit lumen that may hinder protein permeation throughout the network (Gretz et al., 1997). Finally, conduit-independent transport of proteins across the LS endothelium may also contribute to antigen delivery to DCs (Pape et al., 2007). How such factors influence antigen dispersal in LNs and how this intersects with differential positioning and function of DC subsets have not been carefully investigated.

Given the critical importance of LN-resident DCs in the generation of T cell responses to bolus immunizations, with migratory DC subsets playing more substantial roles during highly tropic peripheral infections, such microanatomy-driven processes are likely to have significant ramifications for the generation of adaptive immune responses (Itano et al., 2003; Lee et al., 2009; Hutchison et al., 2012; Woodruff et al., 2014; Gerner et al., 2015; Hor et al., 2015). Further, protein antigens are commonly used in subunit vaccines and can be shed by growing tumors or released by pathogens in the tissue, which emphasizes the importance of acquiring a better understanding of the rules governing antigen biodistribution in LNs and their influence on innate and adaptive immunity (Irvine et al., 2013; Liu et al., 2014; Moyer et al., 2016).

Here, we used two-photon intravital imaging, multiplex confocal microscopy, and histo-cytometry to comprehensively analyze antigen dispersal, uptake, and presentation by DCs, as well as the downstream activation of naive T lymphocytes after protein immunization. We show that the asymmetric distribution of LN-resident cDC1s and cDC2s causes regionalized activation of $CD8^+$ and $CD4^+$ T cells within draining LN, with the $CD8^+$ T cell responses primarily occurring deeper in the LN paracortex, and with $CD4^+$ T cells being preferentially, but not exclusively, activated in peripheral LN regions. Further, we found that although the LN conduits do permit transport of antigens into the deep T cell zone early after immunization, this transport rapidly declines over time, especially in the deep LN paracortex. Extensive conduit-independent antigen dispersal across the floor of the LS establishes steep antigen gradients across the draining LNs. These gradients in turn dominantly determine antigen capture by differentially positioned cDC1 and cDC2 subsets, with the centrally positioned cDC1s capturing significantly less antigen than their LS-proximal cDC2 counterparts. As a consequence, substantially higher doses of administered protein are required for productive MHC I presentation and $CD8^+$ T cell priming, compared with MHC II presentation and $CD4^+$ T cell activation. This steep dose dependence of MHC I presentation has a dramatic effect on the number of $CD8^+$ T cells recruited into the immune response, in turn regulating the response's magnitude and repertoire diversity. Collectively, these findings strengthen the notion that lymphoid tissue microanatomy is intimately involved in regulation of adaptive immunity and suggest that rational antigen design or targeting of specific LN regions with vaccines may promote generation of cell-mediated responses of desired magnitude and quality.

RESULTS

Soluble antigen biodistribution in draining LNs

To investigate the intersection of antigen dispersal after immunization, spatial positioning of DC subsets, and downstream initiation of adaptive immunity in vivo, we initially used two model protein antigens: EαGFP, which allows simultaneous visualization of antigen drainage, uptake, and presentation via MHC II molecules (Itano et al., 2003), and OVA, which permits direct assessment of early T cell activation by monitoring responses of TCR transgenic OVA-specific $CD8^+$ OT-I and $CD4^+$ OT-II T cells.

As previously demonstrated (Roozendaal et al., 2009), two-photon intravital imaging of LNs revealed extremely rapid (1–2-min) drainage of proteins, as well as dextrans, into the LS after s.c. immunization (Video 1). Shortly after initial drainage, we observed substantial conduit-independent entry of antigens into the parenchymal LN space directly across the floor of the LS, consistent with previous studies and ultrastructural observations of the punctuated basement membranes of the LS endothelial barrier (Ohtani et al., 2003; Lämmermann and Sixt, 2008; Gerner et al., 2015). Some of these antigens also appeared to enter the LN conduits, as indicated by association with thin strand-like structures, leading deeper into the paracortex and connecting with the HEVs. Furthermore, visualization of *Itagx*-Venus animals (also known as CD11c-YFP) revealed that some of these soluble antigens were captured by DCs, as indicated by the presence

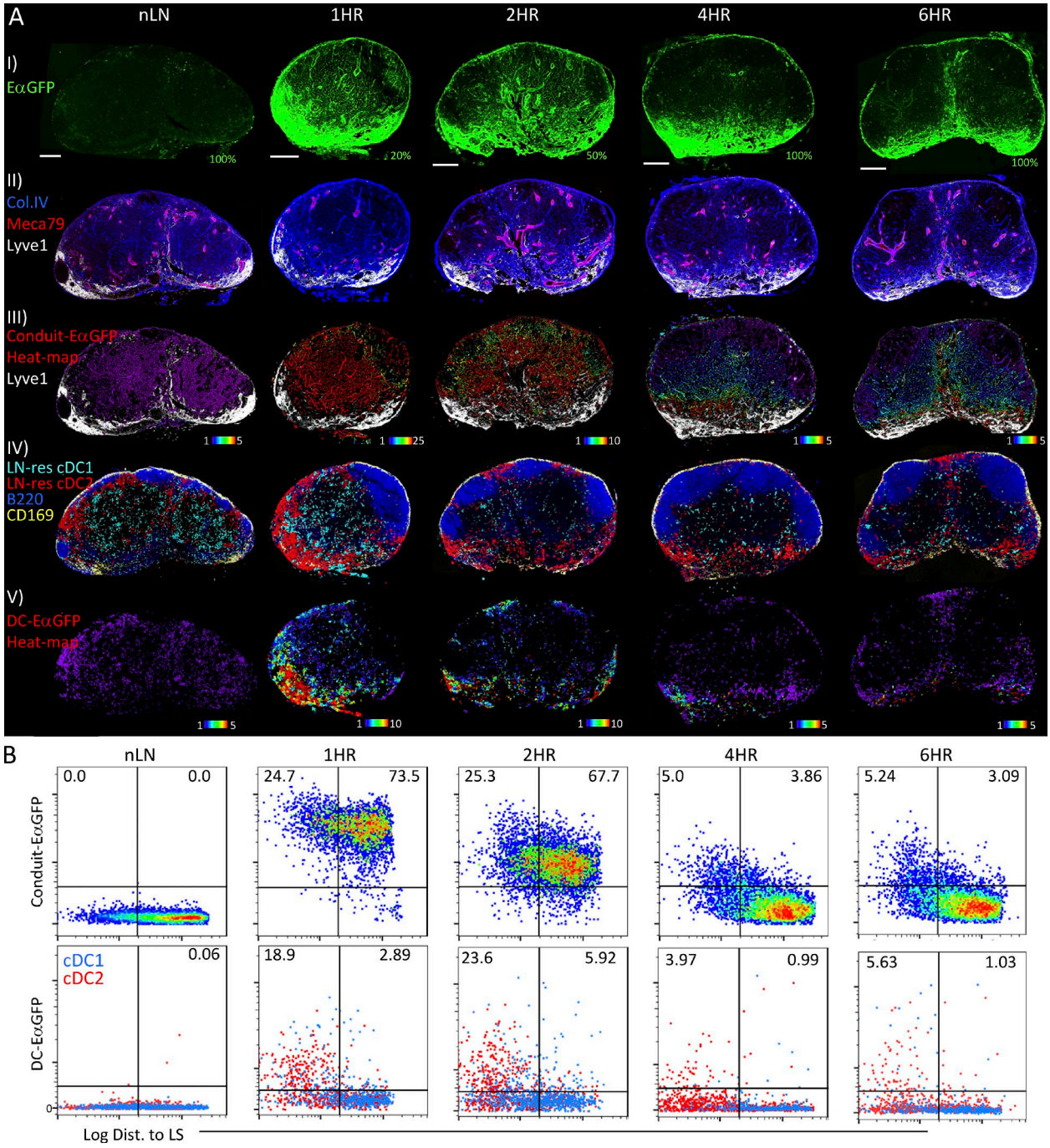

Figure 1. **Soluble antigen dispersal and DC–mediated uptake in LNs.** (A) Mice were injected with EαGFP in the footpad, and draining popliteal LNs were isolated at the indicated time points for visualization of antigen dispersal, as well as uptake by LN-resident DCs. (I) Visualization of the overall EαGFP dispersal across LNs. (II) Identification of stromal elements within LNs, with Lyve-1 (white) signal demarcating the LS, Meca79 (red) staining highlighting the HEVs, and collagen-IV (Coll.IV, blue) staining predominantly denoting the LN conduits. Accompanying gp38 staining of conduits is shown in Fig. S1. (III) Quantitative heat-map analysis of EαGFP signal within conduits, as generated by creating surface objects around LN conduits and quantifying mean EαGFP fluorescence. (IV) Localization of $CD11c^{HIGH}MHC\text{-}II^{INT}CD169^{-}$ LN-resident $SIRPa^{-}$ cDC1 (cyan) and $SIRPa^{+}$ cDC2 (red), with respect to B cells (blue) and $CD169^{+}$ macrophages (yellow). (V) Quantitative heat-map analysis of EαGFP signal within DCs (EαGFP signal gated within $CD11c^{+}Coll.IV^{-}Lyve1^{-}Meca79^{-}gp38^{-}$ voxels). Bars, 200 µm. (B) Conduits (top) and DCs (bottom) from A were quantified for total EαGFP content with respect to distance from the nearest LS. Data represent at least two independent experiments. Numbers in plots represent frequencies.

of dense fluorescent aggregates directly within the cell bodies ofYFP-expressing cells (Video 1).

To examine how such antigens distribute deeper within the LNs, as well as with respect to different DC populations, we used confocal imaging and quantitative histo-cytometry with tissue sections from popliteal and auricular draining LNs isolated at different time points after footpad or ear immunization with EαGFP and stained with various myeloid and stromal cell markers (Figs. 1 A and S1 A). Consistent with the two-photon data, we observed extensive localization of antigen inside the Lyve1$^+$ LS at all examined time points. Some degree of drainage polarity, with heavier labeling of one side of the draining LN, was observed in larger, multilobular LNs (Fig. S1). As anticipated, early after immunization, EαGFP was also detectable within the conduits, as visualized by localization within gp38$^+$collagen-IV$^+$Lyve1$^-$Meca79$^-$, as well as ER-TR7$^+$, thin tubule-like structures within the deeper parenchymal space (Figs. 1 A and S1, A and B). This conduit entry process was molecular weight dependent, as immunization with EαGFP conjugated to a large molecular weight side-chain (allophycocyanin [APC], 105 kD) or use of larger dextrans (>100 kD) led to the inability of such antigens to access the conduits (Fig. S1 B and not depicted). Similar findings were observed in inguinal LNs after s.c. immunization and in the presence of CpG adjuvant (Fig. S1 B and not depicted). We also noted rapid clearance of conduit-associated antigen over time, which was especially apparent within the deeper parenchymal regions, with the vast majority of protein cleared from the centrally localized conduits by 4–8 h after immunization (Fig. 1, A and B; and not depicted). In contrast, LS-proximal conduits maintained a higher degree of labeling even at these extended time points, generating antigen concentration gradients across the conduit network. Collectively, these findings confirm previous observations that small lymph-borne proteins rapidly drain into LNs via the LS and enter the conduit network, while also revealing the extensive conduit-independent dispersal of antigen across the LS endothelium, as well as the nonlinear distribution of such antigens across the LN parenchymal space over time.

Regionalized antigen uptake by DC subsets

To quantitate antigen uptake by different DC subsets, we first used histo-cytometry to identify CD11c^{HI} MHC-II^{INT}CD169$^-$ LN-resident DCs (not depicted) and further subdivide these into the SIRPa$^-$ and SIRPa$^+$, or CD11b$^-$ and CD11b$^+$, cDC1 and cDC2 populations, respectively (Merad et al., 2013;Guilliams et al., 2014). Consistent with our previous findings (Gerner et al., 2012, 2015), LN-resident cDC2s were predominantly localized in close proximity to the LS, whereas the majority of cDC1s localized in the deeper LN paracortex and around the paracortical ridge (Figs. 1 A, S1 A, and S2 A). To ascertain whether such spatial positioning influences antigen uptake, we first gated on internalized EαGFP (EαGFP within CD11c$^+$CD169$^-$gp38$^-$ Col.IV$^-$Meca79$^-$ voxels) and then quantified the mean fluorescence of this DC-associated antigen in differentially localized DCs. This analysis revealed that the vast majority of protein was internalized by the most peripherally positioned DCs at all examined time points, including the early time points when deep T zone conduit-associated antigen was observed (Fig. 1 B), with the peripheral LN-resident cDC2s capturing significantly more antigen than the more centrally localized cDC1s (Fig. 2, A and B; and Fig. S2, B and C). These observations were corroborated with flow cytometry analysis of disassociated cells, which demonstrated similar differences in antigen uptake between cDC1 and cDC2 subsets (Fig. 2, D and E; and Fig. S2 D). Analogous findings were also observed after coadministration of CpG adjuvant, with OVA protein immunization or after dextran injection (Fig. S2, D and F; and not depicted).

These results indicated that the differences in antigen uptake between cDC1s and cDC2s largely correlated with their tissue position and differential antigen accessibility but did not exclude the possibility that intrinsic antigen acquisition capabilities might be responsible for these findings. To examine whether the spatial distribution of DCs or cell-intrinsic differences explained differential antigen uptake, we recalculated the imaging data by examining the mean fluorescence intensity (MFI) of DC-associated antigen only within the LS-proximal cells or by quantifying antigen levels based on overall DC distance from the nearest LS. These analyses demonstrated that the observed differences in antigen uptake between DC populations were negligible if cellular positioning was taken into account (Figs. 2 C and S2 G), suggesting that tissue localization and not intrinsic uptake differences dominantly controlled differential antigen acquisition. In agreement, when isolated from their respective tissue positions and cultured ex vivo, both cDC1s and cDC2s captured similar amounts of protein, with the cDC1s, if anything, being associated with modestly higher levels of EαGFP at the end of the culture (Fig. 2, F and G). Collectively, these data suggest that nonhomogeneous antigen dispersal and asymmetric cellular positioning in draining LNs, and not intrinsic cellular differences, have the greatest impact on in vivo antigen uptake by distinct DC subsets.

Our observations that antigen uptake by DCs was skewed to the LN periphery, regardless of conduit-mediated transport into the deep paracortex (Fig. 1 B), also raised the possibility that conduits may not be essential for delivering antigens to DCs. To examine this in further detail, we quantified the uptake of EαGFP-APC, an antigen too large to enter the conduits, by flow cytometry (Fig. S1 B). This analysis revealed uptake characteristics very similar to those seen with EαGFP, with the cDC1s capturing substantially less antigen compared with cDC2s (Fig. 2, H and I). The overall frequency of DCs capable of capturing EαGFP-APC was only moderately reduced in comparison to EαGFP, and this reduction reached significance only for the cDC1 population (Fig. 2 I). In contrast to DCs and in accord with previous findings (Roozendaal et al., 2009), the frequency of B cells captur-

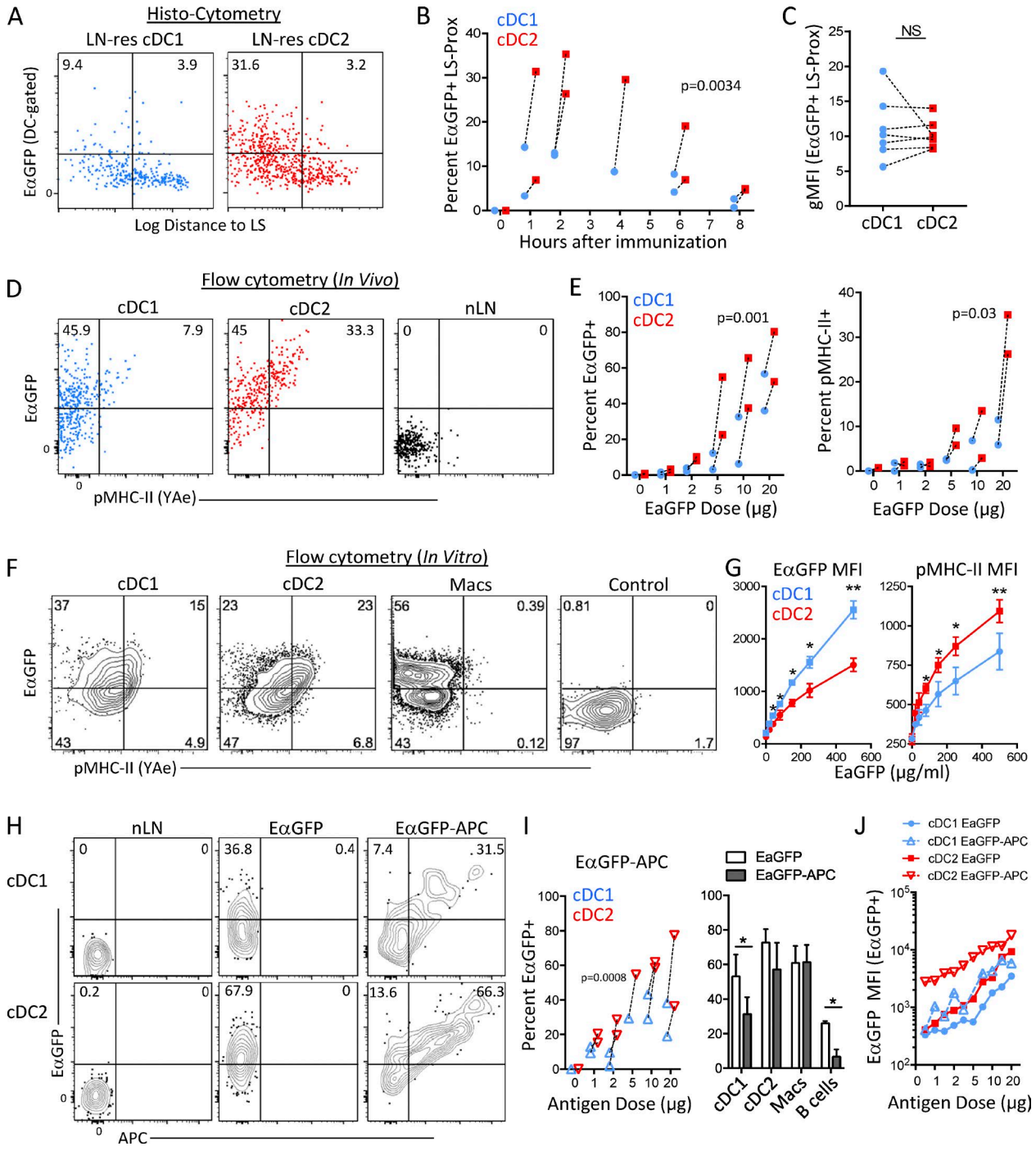

Figure 2. **DC subset positioning influences in vivo antigen uptake and MHC II presentation.** (A–C) Additional quantitative analysis of data presented in Fig. 1. (A) Relative EαGFP uptake by LN-resident cDC1 and cDC2 with respect to distance to the LS in LNs isolated 4 h after immunization. (B) Comparison of the frequency of EαGFP-positive DCs at the indicated time points. (C) EαGFP-positive cDC1 and cDC2 cells located in close proximity to the LS (LS-Prox), as defined by the top left quadrant in A, were examined for the geometric mean fluorescence intensity (gMFI) of EαGFP 1–6 h after immunization. (D and E) Flow cytometry analysis of EαGFP uptake and MHC II presentation (pMHC II) by DC subsets 4 h after immunization. (F and G) Isolated DCs were cultured in vitro with EαGFP for 1 h, washed, and further cultured for 3 h, after which they were examined for EαGFP uptake and MHC II presentation by flow cytometry. (H) Mice were injected with EαGFP or EαGFP-APC, and DC subsets were examined for antigen uptake by flow cytometry. (I) Frequency of antigen-positive cDC1 and cDC2 cells was enumerated (left). Frequencies of antigen-positive DCs, macrophages (Macs), and B cells were compared between EαGFP and EαGFP-APC after administration of 10–20 μg antigen (right). (J) EαGFP MFI was quantified for EαGFP-positive DCs after administration of the indicated quantities of EαGFP and EαGFP-APC antigen. Data represent at least two independent experiments. Dashed lines in B, C, E, and I connect cells within the same draining LNs. Paired *t* test was used for comparing cells within the same LNs. Unpaired *t* test was performed in I. Numbers in flow cytometry and histo-cytometry plots represent frequencies. Error bars are mean ± SD. **, $P \leq 0.01$; *, $P \leq 0.05$; and NS, $P > 0.05$.

ing antigen was significantly influenced by conduit-mediated transport (Fig. 2 I). We also detected a per-cell increase in the total amount of antigen captured by DCs after EαGFP-APC immunization (Fig. 2 J). This appeared to correlate with an apparent increase in EαGFP-APC deposition in the draining LNs, compared with EαGFP (Fig. S1 B), suggesting that conduits may promote clearance of antigens into the circulation and reduce the overall antigen bioavailability in LNs for DCs.

Previous findings on uptake and processing of small soluble antigens by DCs involved use of fluorescent tracers as well as DQ-OVA (Sixt et al., 2005), a modified protein that becomes fluorescent only after proteolytic digestion. Thus, we also used DQ-OVA to investigate the spatial distribution of antigen processing with respect to differentially localized DCs. As reported, we observed substantial fluorescence within the lymphatic endothelium at all examined time points, and some of that signal was also detectable within DCs (Fig. S2 H). Quantitative visualization of DC-associated ($CD11c^+CD169^-Lyve1^-Col.IV^-gp38^-$) DQ-OVA fluorescence revealed a steep distance-to-LS relationship for DQ-OVA processing, with the greatest degree of labeling in DCs localized in close proximity to the LS, and with this signal rapidly decaying with increasing distance from the nearest LS (Fig. S2 H).

Taken together with our data on two-photon visualization of robust conduit-independent antigen dispersal; lack of substantial antigen uptake in central LN regions where conduit-mediated antigen transport is observed at early time points; and normal, if not increased, capture of large molecular weight antigens that are incapable of conduit entry, these findings indicate that conduit-independent antigen dispersal in draining LNs dominantly dictates antigen uptake characteristics by LN-resident DCs.

DC subset positioning influences MHC presentation and T cell priming

LN-resident DCs have been demonstrated to differentially process exogenous antigens for MHC molecule presentation, with the cDC2 subset specializing in MHC II processing and the cDC1 population in MHC I presentation (Dudziak et al., 2007; Merad et al., 2013). How such functional divergence relates to position-dependent antigen uptake and downstream $CD4^+$ and $CD8^+$ T cell responses is not known. To address this question, we first used the EαGFP protein to directly investigate MHC II presentation using a monoclonal antibody recognizing the Eα epitope presented in the context of $I\text{-}A^b$ molecules (Itano et al., 2003). Ex vivo uptake of similar quantities of antigen by both DC populations led to significantly greater peptide–MHC (pMHC) II staining on cDC2s, irrespective of inclusion of adjuvant in the culture medium, confirming their superior intrinsic MHC II processing/presentation capacity (Fig. 2, F and G; and not depicted). In vivo antigen administration also resulted in preferential MHC II presentation by LN-resident cDC2s, regardless of the presence of adjuvant (Fig. 2, D and E; and Fig. S2 D). The greatest pMHC II staining was observed on cells capturing the highest amount of antigen, and these cells were also the cDC2s localized closest to the LS (Fig. 2, A and D; and Fig. S2, B and D). As anticipated, although macrophages took up large quantities of antigen, they failed to efficiently present this protein on MHC II (Fig. 2 F; and not depicted). Furthermore, the relative difference in pMHC II staining between cDC1 and cDC2 populations was markedly accentuated after in vivo antigen administration in comparison to what was observed in the in vitro culture (Fig. S2 E). This indicates that in vivo, a position-dependent increase in antigen accessibility for cDC2s synergizes with their intrinsic efficiency in MHC II processing, leading to overall dominance in MHC II presentation by these cells in comparison to other DC populations.

This relationship of DC position and antigen uptake also suggested that downstream $CD4^+$ T cell responses may be spatially localized to the LN periphery. Conversely, predominant residence of cDC1 within the deeper paracortex may skew MHC I presentation and $CD8^+$ T cell priming to the T cell zone and away from the LS. Because of background staining with the 25D1.16 antibody, which recognizes $OVA^{257\text{-}264}$ peptide bound to H-2Kb, we were unable to robustly detect pMHC I complexes on DCs after OVA immunization. Nevertheless, to ascertain whether DC subset positioning influences the distribution of MHC I versus MHC II presentation and T cell activation, we tracked the location of early $CD8^+$ OT-I and $CD4^+$ OT-II T cell responses shortly after OVA immunization. For this, we took advantage of the fact that when present in sufficiently high numbers, activated T cells rapidly cluster around cells presenting cognate pMHC complexes (Mempel et al., 2004). Thus, regions enriched in $CD8^+$ and $CD4^+$ T cell clusters can provide an in vivo measure of where MHC I and MHC II presentation occurs, respectively. To this end, $\sim 3 \times 10^6$ OT-I and OT-II T cells were transferred into recipient animals to provide an adequate cell number for visualizing such interactions, and the mice were then immunized in the footpad with a high dose of soluble OVA protein. 6–8 h post immunization, draining popliteal LNs were isolated, serially sectioned, and imaged with two-photon microscopy, allowing for visualization of all responding cells in fully reconstructed organs. We observed robust OT-I and OT-II T cell clustering at this high antigen dose, indicating that sufficient antigen was administered for both MHC I and MHC II presentation (Fig. 3 A and Video 2). As noted in previous studies (Eickhoff et al., 2015; Gerner et al., 2015; Hor et al., 2015), $CD4^+$ and $CD8^+$ T cell clusters predominantly occurred as discrete homogeneous aggregates, indicating highly skewed MHC I versus MHC II presentation by the distinct antigen-presenting cells at these early time points. T cell clusters were differentially distributed in LNs, with early $CD8^+$ T cell activation primarily occurring in the deeper LN paracortex. In contrast, $CD4^+$ T cell clusters were frequently, but not exclusively, localized in the peripheral regions proximal to, but not directly within, the LS (Fig. 3, A and B; Fig. S3, A and B; and Video 2). To directly examine whether this early $CD8^+$

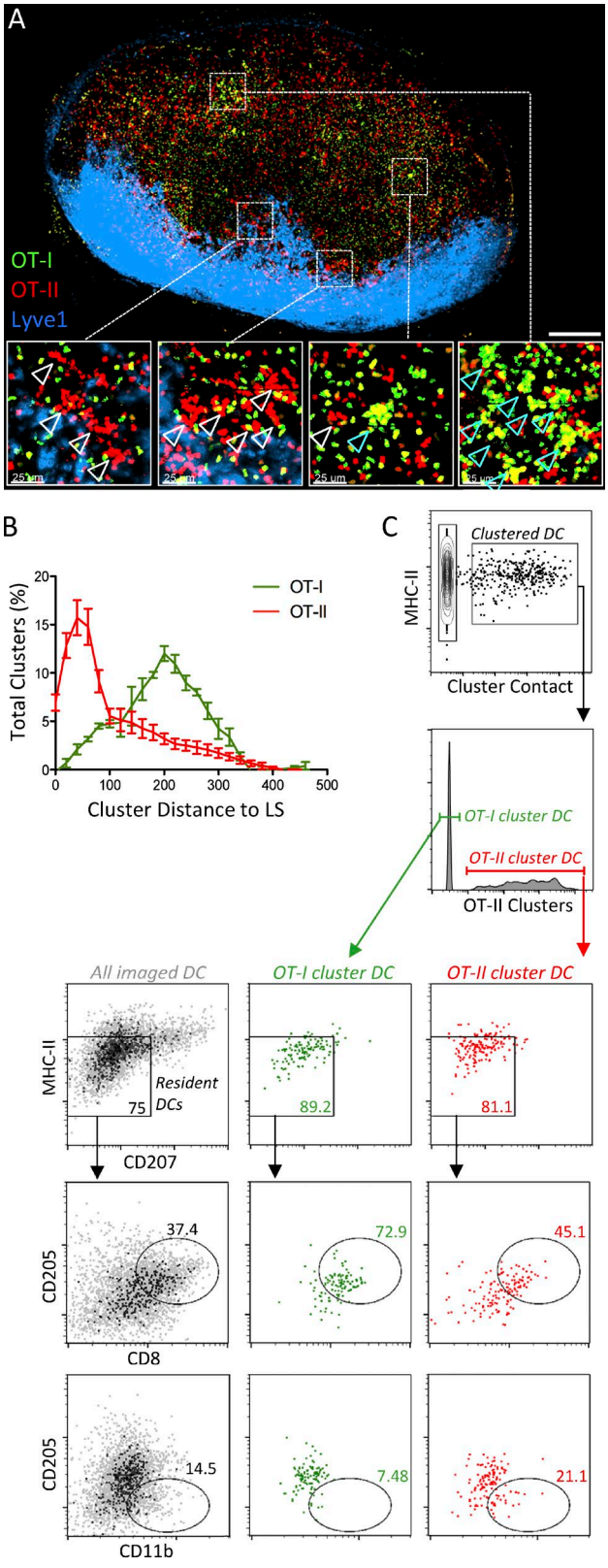

Figure 3. **DC positioning governs the location of MHC I and MHC II presentation and CD8$^+$ and CD4$^+$ T cell activation.** (A) Animals were injected with ~3 × 10^6 OT-I and OT-II T cells labeled with CMFDA (green) and CMTMR (red); 1 d later, they were immunized in the footpad with 10 µg OVA, along with Lyve-1 antibody conjugated to quantum dot 705 for labeling the LS (blue). After 6 h, draining popliteal LNs were isolated, fixed, sectioned into 150-µm slices, and examined with a two-photon 800-nm-wavelength laser for T cell cluster formation (zoom-in insets demonstrate discrete OT-I and OT-II clusters in different areas, as highlighted by cyan and white arrowheads, respectively). Bar, 200 µm. (B) Quantification of the frequency of T cell clusters with respect to the distance to the closest LS. Distance was calculated from the cluster center to the nearest detected Lyve1-stained vessel for all detected clusters. Error bars represent standard error for data from three independent animals. (C) CD45.2$^+$ OT-I and CD45.2$^+$CMTMR$^+$ OT-II T cells were injected into CD45.1$^+$ recipients, which were then immunized with OVA 1 d later. 6 h after immunization, draining LNs were isolated for histo-cytometry analysis of the phenotype of DCs in direct contact with T cell clusters. Numbers in plots represent frequencies. Image analysis pipeline described in Materials and methods. Data represent two independent experiments, three draining LNs per experiment.

and CD4$^+$ T cell activation was mediated by distinct DC subsets, we performed histo-cytometry analysis to quantitatively ascertain the phenotype of DCs in direct contact with clustered T cells (Fig. S3 C; Gerner et al., 2015; Liu et al., 2015; Radtke et al., 2015). This analysis demonstrated that OT-I T cells predominantly clustered around MHC-II^{INT}CD8a$^+$CD205$^+$CD207$^-$ DCs, implicating preferential MHC I antigen presentation by LN-resident cDC1s and not by the migratory CD207$^+$ (CD103$^+$) cDC1s (Figs. 3 C and S3 D). In contrast, OT-II T cell clustering occurred around a mixture of LN-resident cDC1s and cDC2s. These data are consistent with evidence that MHC II presentation can be mediated by a variety of DC populations at sufficiently high antigen doses, albeit with varying efficiencies (Fig. 2, F and G), and with the recent evidence for a key role of cDC1s in the cooperation of CD4$^+$ and CD8$^+$ T cells (Eickhoff et al., 2015; Hor et al., 2015). These clustering data were in agreement with the DC distribution profiles, with positioning of both cDC1s and the corresponding OT-I T cell clusters in central LN regions. Similarly, association of OT-II T cell clusters with multiple DC populations was consistent with the relatively dispersed pattern of OT-II cluster distribution, with only partial enrichment in the LS-proximal regions inhabited by LN-resident cDC2s. Collectively, these findings indicate that DC subset positioning in LNs generates regions that are specialized in MHC I and MHC II presentation and downstream activation of CD8$^+$ and CD4$^+$ T lymphocytes.

Differential antigen dose requirements for MHC I and MHC II presentation

Considering the nonequivalent dispersal of antigens across LNs, we next hypothesized that substantially higher doses of administered antigen would be necessary for the more centrally localized cDC1s to elicit CD8$^+$ T cell activation, compared with the peripheral CD4$^+$ T cell activation by cDC2s, especially given the relative inefficiency of cross-presentation (Savina and Amigorena, 2007; Alloatti et al., 2016). To address

this possibility, we titrated the amount of administered OVA protein and examined early OT-I and OT-II T cell responses, as assessed by surface levels of CD69 and CD62L, two markers of early T cell activation. High-dose immunization conditions elicited robust activation of both T cell populations (Fig. 4, A and B; and Fig. S4 A). In contrast, lowering the antigen dose preferentially decreased the frequency of activated OT-I T cells, while only moderately affecting OT-II T cell priming. These differences were corroborated with cluster formation experiments, which also demonstrated greater sensitivity of OT-I T cell clusters, compared with OT-II T cells, to low-dose antigen administration (Fig. 4 C). The greatest decline in OT-I T cell clustering was observed in regions located distal to the LS, indicating that these regions were most susceptible to antigen dose modulation. In contrast, the greatest decline in OT-II T cell clustering occurred in LS-proximal regions (Fig. 4 D). We further ascertained whether conduit-mediated antigen transport was involved in differential $CD4^+$ versus $CD8^+$ T cell activation by immunizing animals with OVA-APC conjugate, an antigen that would be too large to enter the LN conduits. In agreement with the EαGFP-APC uptake data (Fig. 2 I), we observed a similar difference between OT-I and OT-II T cell activation in response to different doses of antigen as was seen with OVA, indicating that conduit-mediated antigen delivery is not critical for differential $CD4^+$ vs. $CD8^+$ T cell priming by DCs (Fig. S4, B and C).

The simplest interpretation of these findings is that in vivo, the capacity of antigens to reach differentially localized DC populations within draining LNs dictates the extent of pMHC display and the resulting T cell subset stimulation. An alternate explanation to this model could involve differences in the relative efficiency of MHC-specific antigen-processing efficiency, with greater total antigen uptake by DCs being necessary for MHC I compared with MHC II presentation (Savina and Amigorena, 2007). Previous ex vivo T cell priming studies, where both cDC1 and cDC2 populations took up equivalent amounts of antigen, demonstrated either similar or enhanced activation of OT-I compared with OT-II T cells (Schnorrer et al., 2006; Kamphorst et al., 2010). These data argue that $CD8^+$ and $CD4^+$ T cell activation can both occur at similar antigen doses, provided that all DC populations have equivalent access to antigen. To directly examine whether normalization of antigen uptake by DC populations would lead to comparable in vivo OT-I and OT-II activation, we isolated lymphoid-tissue DCs, pulsed them ex vivo with varying doses of OVA, and then injected these cells s.c. into recipient animals. Splenic DCs were used for this experiment to obtain sufficient number of cells for immunization, and these DCs showed relatively similar in vitro antigen uptake characteristics as LN-derived cells (not depicted). 18 h later, after OVA-pulsed DCs had sufficient time to migrate to LNs, these animals were administered naive OT-I and OT-II T cells. 12–14 h later, immunized LNs were harvested and examined for T cell priming via microscopy. We observed robust T cell cluster formation, suggesting that efficient T cell activation was occurring with this DC immunization model (Fig. S4 D). Nearly identical frequencies of activated OT-I and OT-II T cells were observed after pulsing DCs with low amounts of OVA, suggesting that MHC I and MHC II presentation can both occur at similarly low antigen doses, provided that all DC populations capture comparable amounts of antigen (Fig. S4 E). Although higher OVA pulsing conditions resulted in moderately better OT-II T cell priming, this likely reflected the intrinsic capacity of all DC subsets for MHC II presentation given sufficiently high antigen, whereas only the cDC1 appear capable of MHC I processing.

A second alternative explanation for our results was that differing affinities of OT-I and OT-II T cell TCRs toward their cognate pMHC complexes were contributing to the discrepancy in T cell activation after low-dose antigen administration (Stone et al., 2009; Mandl et al., 2013). However, OT-I T cells have a reportedly higher overall avidity as compared with OT-II T cells (Surh and Sprent, 2008), which is inconsistent with the observed results. Nevertheless, we used a distinct TCR transgenic T cell pair, P14 $CD8^+$ and Smarta $CD4^+$ T cells, both of which recognize lymphocytic choreomeningitis virus glycoprotein (GP) presented on the respective MHC molecules. As anticipated, immunization with high doses of GP led to efficient activation of both T cell populations. Similar to the OT-I and OT-II T cell system, lowering antigen doses led to a rapid decrease in the frequency of activated $CD8^+$ P14 but not $CD4^+$ Smarta T cells (Fig. 4, E and F). These data argue that the differential in vivo activation of $CD8^+$ and $CD4^+$ T cells in limiting antigen conditions is not dominantly dictated by TCR avidity, although this may of course also contribute to the nature of the T cell response.

Polyclonal T cell responses to varying antigen dose administration

How do observations obtained with thousands to millions of adoptively transferred cells relate to more physiological immunization conditions where a few dozen naive polyclonal precursor T cells have to find their cognate pMHC complexes presented on DCs (Jenkins and Moon, 2012)? One possibility is that similar to the change in frequency of activated TCR transgenic cells, varying the amount of administered antigen would result in different numbers of naive endogenous T cells recruited into the immune response. This in turn would likely be linked to a change in the response's clonal diversity, as well as its overall magnitude. To address this issue, we immunized animals in the footpad with varying doses of recombinant GP along with CpG and, 8 d later, examined the endogenous polyclonal $CD4^+$ and $CD8^+$ T cell responses in the spleen using MHC tetramer staining (Fig. 5 A). GP was used in these studies, as this antigen allowed robust detection of both $CD4^+$ and $CD8^+$ responses with tetramers (see next section). We observed well-defined responses after high-dose antigen immunization for both $CD4^+$ and $CD8^+$ T cells. In contrast, lowering the amount of administered antigen resulted in a

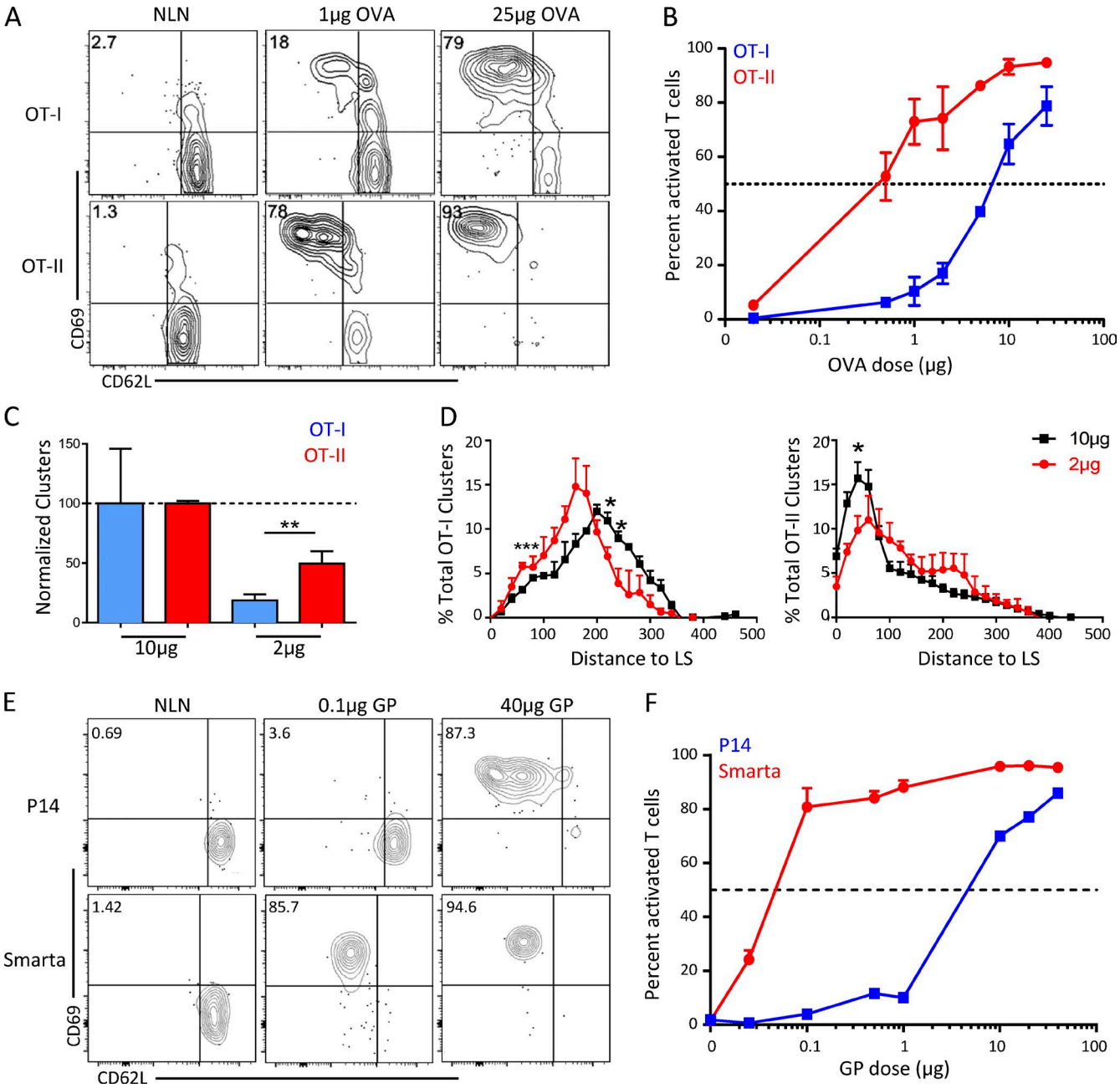

Figure 4. **Differential antigen dose requirements for early CD8⁺ and CD4⁺ T cell activation.** (A and B) Mice were injected with ∼0.75 × 10^6 OT-I and OT-II T cells and 1 d later immunized with the indicated doses of OVA. 12 h later, draining LNs were examined for the expression of CD69 and CD62L on transferred T cells by flow cytometry (A), with the percentage activated T cells ($CD69^+CD62L^-$) quantified across individual animals (n = 4; B). (C) The same experimental procedure as in Fig. 3 A, examining the relative OT-I and OT-II T cell cluster formation after low-dose (2 µg) OVA immunization. Data were normalized to T cell cluster formation after high-dose (10 µg) OVA immunization. (D) Extended dataset of experiment presented in Fig. 3, examining the relative distribution of OT-I and OT-II T cell clusters with respect to distance to the nearest LS after low-dose (2 µg) or high-dose (10 µg) antigen administration. Error bars are mean ± SEM. (E and F) Mice were injected with ∼0.5 × 10^6 P14 and Smarta T cells and immunized with the indicated doses of GP. 12 h after immunization, draining LNs were examined for expression of CD69 and CD62L on transferred T cells by flow cytometry (E), with the percentage activated T cells quantified across different animals (F). Data represent at least two independent experiments. Numbers in flow plots represent frequencies. Error bars are mean ± SD, unless otherwise indicated. ***, P ≤ 0.001; *, P ≤ 0.05.

striking reduction of $CD8^+$ T cell priming, while still maintaining potent $CD4^+$ T cell responses (Fig. 5 B). Although spleens were used here to improve detection of expanded, recirculating effector T cells at late time points, as well as to obtain sufficient sample to examine the repertoire diversity of this effector T cell pool, a similar divergence in $CD4^+$ and $CD8^+$ T cell responsiveness to antigen dose manipulation was observed in draining LNs after blocking the effector cells' capacity to recirculate with FTY720 (Fig. S5, A–C). Moreover, this differential T cell priming was largely independent of migratory DC involvement, as immunization conditions in which antigen presentation was restricted to LN-resident DCs via injection site removal (Itano et al., 2003; Gerner et al., 2015) led to similar results (Fig. S5, A–C). We next examined the clonal diversity of the expanded GP-specific $CD4^+$ and $CD8^+$ T cells by analyzing the Vb gene usage of tetramer binding cells by flow cytometry (Fig. 5 A). This technique revealed individual Vb families contributing to the composite T cell responses (Fig. 5 C). We found that $CD4^+$ T cells generated highly diverse response repertoires at all examined antigen doses, and importantly, this diversity was significantly greater than that of $CD8^+$ T cell responses (Fig. 5 D).

We next attempted to study endogenous T cell responses to a second antigen, OVA, although in contrast to GP, OVA immunization resulted in poor signal-to-noise characteristics of MHC II OVA tetramer staining (not depicted). Nevertheless, robust detection of OVA-specific $CD8^+$ T cell responses was observed with high-dose (25 µg) OVA administration (Fig. 5 E). Reducing the dose of administered OVA by 100-fold (0.25 µg) also reduced the total magnitude of the resultant $CD8^+$ T cell responses (Figs. 5 E and S5 D), and not all of the low-dose OVA immunized animals mounted a detectable response. This suggested that the low-dose OVA immunization conditions were operating at the lower limit of sensitivity for effective MHC I presentation and $CD8^+$ T cell activation. Of the animals that did respond, we observed relatively similar IFNγ production after restimulation, as well as expression of various markers of differentiation for both low- and high-dose conditions, suggesting that comparable effector differentiation was taking place (Fig. S5 E). As above, we next examined the repertoire diversity of expanded OVA-reactive $CD8^+$ T cells. High-dose OVA administration led to substantial response representation by most Vb families in all examined animals, suggesting that sufficient antigen was delivered to elicit efficient activation of a large number of naive $CD8^+$ T cells and a highly diverse resultant clonal repertoire. In contrast, low-dose OVA immunization resulted in severely limited Vb familial representation, suggesting restricted clonal diversity (Figs. 5 F and S5 F). These results indicate that antigen dosage is a limiting factor to the repertoire diversity of $CD8^+$ T cell responses.

The majority of detected $CD8^+$ T cell Vb families, in both low- and high-dose OVA immunization conditions, had relatively similar magnitudes of overall clonal expansion (Fig. S5 G). Further, the magnitudes of individual $CD8^+$ T cell familial clonal bursts were relatively similar between the low-dose OVA and GP-specific responses, although a minor difference was detected between GP and high-dose OVA immunization (Fig. S5 G). Although some variation was detected between different families within a given $CD8^+$ T cell response, in accordance with previous literature (Obst, 2015), these results argued that once activated, individual $CD8^+$ T cells undergo a similar extent of proliferation, regardless of antigen dose. This also indicated that the overall magnitude of $CD8^+$ T cell responses to subunit antigen immunization is in large part determined by the total number of naive T cells recruited into the response, rather than dictated by the preferential expansion of individual cells upon activation, as was reported for infection settings (Buchholz et al., 2013; Gerlach et al., 2013). Indeed, we found a strong linear correlation between the number of Vb families participating in the OVA- and GP-specific $CD8^+$ T cell responses and the overall magnitude of the resultant response (Fig. 5 G). Such correlation was less obvious for MHC II restricted $CD4^+$ T cells (Fig. S5 H), indicating that the magnitude of $CD4^+$ T cell responses is set by distinct factors than for $CD8^+$ T cells. Collectively, as with our adoptive transfer experiments (Fig. 4), these data indicate that polyclonal $CD8^+$ T cell responses necessitate administration of substantially higher doses of antigen than for generation of $CD4^+$ T cell responses, arguing that limited antigen availability for cross-presenting cDC1s directly influences the diversity and in turn the magnitude of the resultant $CD8^+$ T cell responses.

DISCUSSION

Generation of adaptive immunity is dependent on effective capture and presentation of foreign antigens by DCs. This can be mediated via two independent mechanisms: rapid drainage of lymph-borne antigens from peripheral tissues into LNs, followed by localized uptake and presentation by LN-resident DCs, or via peripheral tissue antigen uptake and delayed active transport by migratory DCs (Cyster, 2010). The precise contributions of these pathways are context dependent. Early drainage of antigens to the LN promotes rapid induction of cellular and humoral adaptive immunity and plays critical roles in host defense (Allenspach et al., 2008; Lee et al., 2009; Cyster, 2010; Gonzalez et al., 2010; Anandasabapathy et al., 2014; Woodruff et al., 2014; Eickhoff et al., 2015; Gerner et al., 2015; Hor et al., 2015). Although migratory DC populations are important for T cell activation during highly tropic or slow-replicating infections, they do not seem to be essential for efficient initiation of either $CD4^+$ or $CD8^+$ T cell responses to bolus immunizations (Itano et al., 2003; Lee et al., 2009; Hutchison et al., 2012; Woodruff et al., 2014; Gerner et al., 2015; Hor et al., 2015). Thus, understanding the rules guiding early antigen drainage, dispersal within LNs, and downstream induction of innate and adaptive immunity by LN-resident DCs is critical for effective design of vaccines and immunomodulatory therapeutics (Irvine et al., 2013; Moyer et al., 2016).

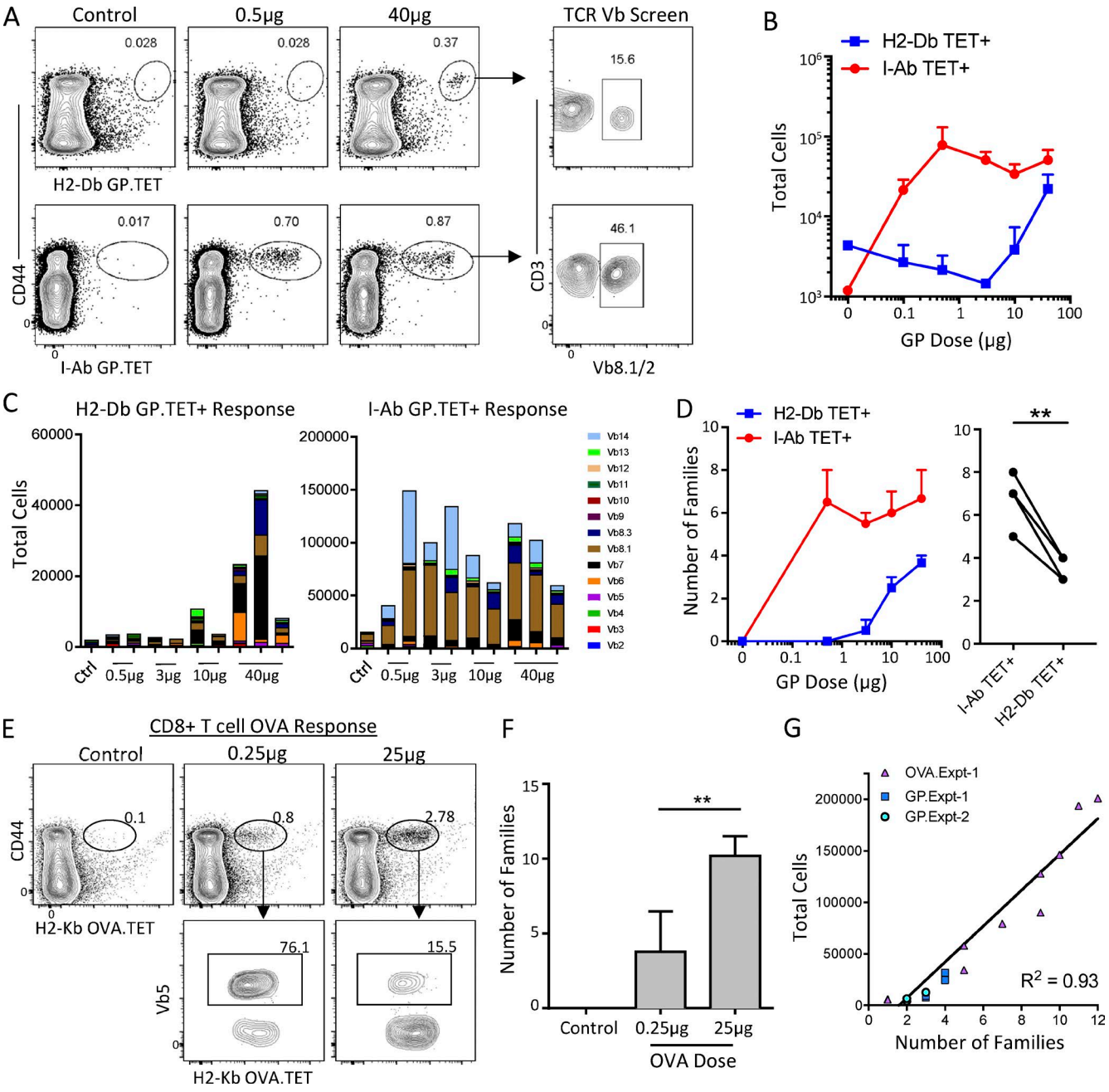

Figure 5. **Antigen dose–dependent regulation of polyclonal CD4⁺ and CD8⁺ T cell responses.** (A) Mice were immunized in the footpad with indicated doses of recombinant GP along with CpG; 8 d later, spleens were examined for presence of H2-Db GP.Tetramer⁺ (GP.TET) CD8⁺ T cells and I-Ab GP.TET⁺ CD4⁺ T cells by flow cytometry. Tetramer⁺ cells were also examined for Vb2-14 staining (Vb8.1/2 demonstrates representative staining). (B) Enumeration of the total number of I-Ab GP.TET⁺ CD4⁺ and H2-Db GP.TET⁺ CD8⁺ T cells after immunization with the indicated doses of GP and CpG. Error bars are mean ± range. (C) Analysis of the Vb repertoire of the tetramer⁺ T cells. Bars indicate individual animals. (D) Enumeration of the total number of Vb families contributing to the CD4⁺ (I-Ab TET⁺) and CD8⁺ (H2-Db TET⁺) T cell responses to GP. Error bars are mean ± range. Paired *t* test was performed comparing the familial representation within the CD4⁺ versus CD8⁺ T cell response within the same mice. GP immunization data represent two independent experiments. (E) Mice were immunized with low (0.25 µg) or high (25 µg) doses of OVA protein along with CpG, and 7 d later spleens were examined for presence of H2-Kb OVA. TET⁺ CD8⁺ T cells. (F) Enumeration of the mean number of Vb families contributing to the total OVA-specific CD8⁺ T cell response. Mice lacking detectable responses (0.25 µg dose group) were excluded from analysis. Error bars are mean ± SD; $n = 5$. OVA immunization data represent at least three independent experiments. (G) Correlation analysis comparing the total number of Vb families participating in a given response and the total number of antigen-specific CD8⁺ T cells within that response. Responses against GP and OVA antigens were combined for analysis. For analyses of relative familial composition (D, F, and G), control nonimmunized samples were first used to determine the maximum potential contribution of nonspecific events in the Tetramer⁺ gates, and this value was used as a cutoff to enumerate the number of true responder families. Numbers in flow plots represent frequencies. **, $P \leq 0.01$.

Here, we used a subunit protein immunization model to reveal direct relationships between architecturally determined soluble antigen dispersal, steady-state DC subset positioning, location-dependent antigen uptake, and the downstream activation of $CD8^+$ and $CD4^+$ T lymphocytes. Specifically, we found that the overall proximity of DC populations to the LS dominantly dictates the amount of antigen they can capture. This appears to be in large part because of nonhomogeneous antigen dispersal across the LN parenchyma, with dramatically lower amounts of antigen within the deep T cell zone. This distribution appears to be largely generated through conduit-independent dispersal of proteins across the floor of the LS into the parenchymal space. Although the conduit network does permit early transport of small molecular weight antigens into the deep T cell zone, at least in our hands, such conduit transport did not appear critical for delivering antigens to DCs or for the induction of T cell responses. Importantly, the parenchymal antigen gradients have direct consequences for uptake by the differentially positioned DC subsets, with the more centrally localized LN-resident cDC1 capturing significantly less protein than the LS-proximal LN-resident cDC2 population. Because of the relative specialization of these DC subsets for MHC I versus MHC II presentation (Merad et al., 2013), the discrepancy in antigen uptake in turn leads to significant differences in the amount of administered antigen necessary for $CD4^+$ versus $CD8^+$ T cell activation, with $CD8^+$ T cells requiring substantially greater doses for the generation of responses. In this fashion, microanatomically determined antigen access of LN regions specialized for MHC I versus MHC II presentation directly governs the efficiency of $CD8^+$ versus $CD4^+$ T cell recruitment into the response, controlling the magnitude and repertoire diversity of downstream cellular adaptive immunity.

LN conduits, laid down and ensheathed by fibroblastic reticular cells, consist of a central, fluid-filled luminal region that contains collagen fibers and other extracellular matrix proteins (Gretz et al., 1997; Lämmermann and Sixt, 2008; Roozendaal et al., 2008). Small soluble molecules (<70 kD) can rapidly access this conduit lumen and penetrate deeper into the paracortical regions of the LN for potential sampling by LN-resident DCs (Gretz et al., 1997; Sixt et al., 2005; Rantakari et al., 2015). Early studies demonstrated relatively poor penetration of tracer dyes into the deep T cell zone, suggesting nonuniform dispersal of antigens across draining LNs (Sixt et al., 2005). Our histo-cytometry image analysis extends these studies by demonstrating clear filling of conduits within the deep T cell zone early after immunization. However, this is short-lived, and intraconduit antigen levels rapidly dissipate over time, especially in these deep LN regions, suggesting that the vast majority of these proteins are transported into the circulation. Some antigen does continue to be detected at higher concentrations in conduits proximal to the LS, indicating that low-grade conduit filling continues to occur in the LN periphery even at late time points.

Beyond these conduit-related events, our two-photon intravital imaging studies demonstrated extensive conduit-independent penetration of parenchymal tissue space by administered antigens, likely involving direct molecular diffusion and bulk fluid movement across the heavily fenestrated basement membranes of the LS endothelium (Pape et al., 2007; Lämmermann and Sixt, 2008; Roozendaal et al., 2009). Dispersal of antigens within the LN parenchyma was also likely promoted by lymphocyte motility, which can promote mixing of these interstitial fluids and antigens in the LN. In concert with the late conduit-based filling, these diffusive processes generated steep antigen gradients across the LN parenchymal space after immunization, with significantly greater antigen abundance in the regions most proximal to the LS. As a consequence, this nonlinear antigen dispersal appeared to directly influence antigen uptake by the differentially positioned DC subsets, with the more centrally localized LN-resident cDC1 capturing significantly less protein than the LS-proximal cDC2 population. Although previous work suggested a conduit dependence of DC-mediated antigen uptake as well as preferential antigen processing by differentially localized DC subsets, this study did not use antigen size restriction to directly ascertain the role of conduit transport in DC antigen presentation activity (Sixt et al., 2005). Our data now indicate that conduits play a limited role in delivering antigens to DCs, as large proteins unable to enter conduits promoted similar DC uptake, and if anything, increased the total amount of antigen per cell. T cell responses were also maintained using conduit-inaccessible antigen. These data indicate that conduit-independent dispersal dominantly determines antigen capture and processing by DCs. We would thus like to speculate that the predominant physiological function of LN conduits is to promote fluid equilibration with respect to interstitial and blood circulatory systems, allowing rapid return of lymph fluids, and associated small antigens, into the circulation. On an immunological level, conduits are also likely critical for allowing small inflammatory mediators and chemokines to access and decorate the vascular endothelium in draining LNs, as previously shown (Baekkevold et al., 2001; Palframan et al., 2001).

We also generated a direct link between the location-based antigen uptake by different DC subsets with their unique functional roles in generation of T cell responses. First, our DC–T cell cluster contact studies validated the selective capacity of LN-resident cDC1s to present antigens on MHC I molecules. Further, we demonstrated the propensity, but not exclusivity, of LN-resident cDC2s to present antigens on MHC II molecules and induce $CD4^+$ T cell priming. Similar to our earlier observations (Eickhoff et al., 2015), the spatial segregation of these DC subsets in turn influenced the location of where $CD8^+$ and $CD4^+$ T cells were likely to see their cognate antigens, with preferential early activation of $CD8^+$ T cells within the deeper LN paracortex and the tendency of $CD4^+$ T cells to be activated in more LS-proximal regions. Because of the nonlinear antigen dispersal in LNs, the relatively poor uptake by the deep paracortical cDC1s resulted in limited MHC I presentation, permitting robust $CD8^+$ T cell

activation only after administration of high doses of antigen. In contrast, peripheral localization of LN-resident cDC2s promoted capture of greater quantities of antigen, which synergized with their intrinsic propensity toward MHC II processing, and allowed these DCs to maintain $CD4^+$ T cell activation even during limiting antigen conditions.

Why would the immune system be designed in such a way, inducing selective T cell responses based on antigen dose availability and allowing robust $CD8^+$ T cell priming only in conditions of large protein abundance? One answer may lie in the likely natural roles of T cells in immunity. The primary evolutionary role for cytotoxic $CD8^+$ T lymphocytes is considered to be protection against intracellular pathogens, which are not likely to produce copious amounts of lymph-borne soluble antigens, although some proteins would certainly be released from infected or dying cells (Laidlaw et al., 2016). Activation of $CD8^+$ T cells in such scenarios would be predominantly mediated either through microbial infection of permissive host cells and direct presentation of cytosolic proteins, or via trafficking of infected DCs to draining LNs for antigen hand-off to LN-resident cDC1s (Eickhoff et al., 2015; Groom, 2015; Hor et al., 2015; Kitano et al., 2016). Indeed, we as well as other groups have previously demonstrated that tissue-derived DCs migrate into the deep paracortex of the LN, with distinct subsets further segregating between the inner T cell zone and interfollicular regions (Kissenpfennig et al., 2005; Gerner et al., 2012; Kitano et al., 2016). Predominant positioning of LN-resident cDC1s in these same regions may thus be strategically optimized for efficient interception of migratory cells carrying infectious agents (Heath and Carbone, 2009; Hor et al., 2015). In a similar fashion, the ∼30% of cDC1s that do localize in closer proximity to the LS may be functionally predisposed to sample locally dying cells from their local microenvironments after lymph-borne lytic infections (Gerner et al., 2012; Eickhoff et al., 2015; Kitano et al., 2016). These considerations are also consistent with evidence that cell-associated antigens, which would be encountered after lytic infection, are superior to soluble proteins for accessing the cross-presentation pathway (Li et al., 2001).

In contrast, early $CD4^+$ T cell activation with subunit antigen immunization not only appears to be elicited on a different DC platform, but also occurs at significantly lower antigen doses than for $CD8^+$ T cells. Functionally, lowering the antigen dose requirement may potentiate the critical roles of $CD4^+$ T cells as helper cells, allowing a larger number of activated $CD4^+$ T cells expressing CD40 ligand to embark on a migratory journey and search for secondary interactions with activated B cells or cross-presenting cDC1s (Eickhoff et al., 2015).

The nature of lymph-borne soluble proteins in steady-state conditions must also be considered in attempting to understand the spatial segregation of antigen-presenting cells. These are mainly composed of tissue-derived self-antigens and serum proteins (Hansen et al., 2015). It is tempting to speculate that limited MHC I presentation of such antigens by centrally positioned cDC1 minimizes the likelihood of autoreactive activation of $CD8^+$ T cells (Kurts et al., 1998). In contrast, positioning of LN-resident cDC2 proximally to the LS may promote steady-state MHC II presentation of endogenous antigens to $CD4^+$ T cells and induction of peripheral tolerance. As an additional safety checkpoint, separation of early MHC I and MHC II presentation on distinct DC populations and in different spatial compartments would further reduce the likelihood for accidental provision of $CD4^+$ T cell help during potential autoreactive $CD8^+$ T cell reactions. Further control of such self-specific responses in steady-state conditions can be efficiently provided by localized activity of regulatory T cells (Liu et al., 2015).

Our findings are of significant relevance to vaccine development, providing a mechanistic understanding of how antigen dispersal influences innate and adaptive immune responses. Subunit protein vaccines have generally failed to yield protective $CD8^+$ T cell immunity, although still generating competent $CD4^+$ T cell and humoral responses (Koup and Douek, 2011; Pennock et al., 2016). In addition to previous indications that soluble antigens are inefficiently targeted to the cross-presentation pathway, our data now reveal that the relatively poor capacity of administered protein antigens to reach the DCs specialized in cross-presentation is a major limiting step in generation of potent $CD8^+$ T cell immunity. Antigens that are retained better within LNs, while also having higher diffusive properties, may promote stronger $CD8^+$ T cell responses. This is consistent with observations that certain particulate vaccine formulations can promote long-term antigen persistence in draining LNs and augment the $CD8^+$ T cell response (Kastenmüller et al., 2011; Liu et al., 2014; Lynn et al., 2015). These new data also make sense with respect to additional immunization strategies used to optimize the $CD8^+$ T cell response. Antibody-based antigen targeting that selectively targets cross-presenting DCs is likely to work through diffusive processes, as these antigens are too large to access the conduit network (Tacken et al., 2007; Kastenmüller et al., 2014; Lehmann et al., 2016). On the other hand, live viral vectors or liposomal formulations are likely to work by completely bypassing the requirements of cross-presentation by cDC1s. It is important to point out that recent studies have demonstrated that multiple DC populations can cross-present antigens if they are captured via receptor-mediated endocytosis (Kamphorst et al., 2010; Cohn and Delamarre, 2014). Thus, it is possible that prime-boost vaccinations that elicit antibody production and formation of immune complexes may promote broader DC involvement in cross-presentation.

Finally, our data indicate that the magnitude of $CD8^+$ T cell responses to subunit immunization is largely proportional to the overall repertoire diversity of cells recruited into the response. This is different from observations made in bacterial and viral infection settings, in which preferential proliferative expansions of individual T cell clones can dominantly determine a response's magnitude, and is likely a result of the much more homogeneous priming conditions experienced

by $CD8^+$ T cells after bolus subunit vaccination compared with i.v. infection (Buchholz et al., 2013; Gerlach et al., 2013). Although these results may vary in conditions of repeated antigen exposure after boosting, this indicates that initial recruitment of large number of naive $CD8^+$ T lymphocytes is essential for generation of $CD8^+$ T cell responses of optimal magnitude and diversity (Tscharke et al., 2015). Increased response diversity would in turn promote better protection against potential escape mutations arising during viral infections and in cancer (Nikolich-Žugich et al., 2004; van der Burg et al., 2016). In contrast to the burst-like proliferation of naive $CD8^+$ T cells, with the total effector pool predominantly set by the number of recruited cells, $CD4^+$ T cell responses appear to be less guided by clonal recruitment, likely representing the previously shown requirements for continued stimulation by antigen-presenting cells for maximal generation of responses (Celli et al., 2005; Obst et al., 2005).

The combination of intravital two-photon imaging and highly multiplex immunohistochemical analysis has reemphasized the central role that tissue microanatomy plays in immune function. As imaging tools and detection probes have improved, additional layers of topographic complexity within secondary lymphoid tissues have emerged along with clear evidence that the fine-grained distribution of immune cell populations is critical to innate and adaptive host defense (Cyster, 2010; Gerner et al., 2012, 2015; Kastenmüller et al., 2012; Qi et al., 2014; Groom, 2015; Lian and Luster, 2015; Liu et al., 2015). Here we provide a direct link between the spatial organization of lymphoid tissues and the generation of cell-mediated adaptive immune responses, findings that also identify critical elements for consideration with regard to rational vaccine design.

MATERIALS AND METHODS

Mice

$CD45.1^+$ C57BL/6, *Itgax*-Venus (CD11c-YFP), C57BL/6 OT-II, OT-I, and P14 TCR transgenic mice were obtained from Taconic Laboratories (Pircher et al., 1989; Hogquist et al., 1994; Barnden et al., 1998; Lindquist et al., 2004). Smarta $CD4^+$ T cell transgenic animals were provided by E. Shevach (National Institutes of Health, Bethesda, MD; Oxenius et al., 1998). Actin-eCFP mice were obtained from The Jackson Laboratory. 6–10-wk-old male and female mice were maintained in specific pathogen–free conditions at an Association for Assessment and Accreditation of Laboratory Animal Care–accredited animal facility at the National Institute for Allergies and Infectious Diseases (NIAID). Animals were randomly allocated into treatment groups. The investigators were not blinded to allocation during experiments and outcome assessment. All procedures were approved by the NIAID Animal Care and Use Committee (National Institutes of Health).

BM chimeras

Actin-eCFP animals were exposed twice to 600 rad of gamma irradiation from a cesium source separated by a 3-h rest period. 5×10^6 total donor CD11c-YFP BM cells were injected i.v. the same day. Mice were rested and given neomycin or sulfamethoxazole water for 4 wk and used experimentally 6–10 wk later.

Adoptive transfers

Naive ($CD44^{low}$) T cells were purified from LN and spleen tissues with negative selection T cell isolation kits (Miltenyi Biotec), with the antibody cocktail supplemented with 1:10,000 biotinylated CD44 antibody to deplete memory cells. For imaging studies, cells were differentially labeled with 1 µM CellTracker Green CMFDA and 1:10 pluronic polyol :dye ratio (Invitrogen) or 10 µM CellTracker Orange CMTMR (Invitrogen) in 10% FCS complete RPMI (cRPMI). After 15 min of labeling at 37°C, cells were washed and rested for 30 min in cRPMI, washed with PBS, and transferred into $CD45.1^+$ C57BL/6 hosts.

Antigen fate and immunization studies

For antigen distribution and uptake studies, indicated quantities of EαGFP, a gift from M. Jenkins (University of Minnesota, Minneapolis, MN), along with 25 µg CpG 1668 (Trilink Biotech) where indicated, in PBS (20 µl final volume) were injected in the footpad or the ear pinnae. In certain experiments, EαGFP conjugated to APC (Innova Biosciences) was used. In some studies, OVA-Alexa Fluor 488 protein, a gift from Y. Belkaid (National Institutes of Health) or fluorescently labeled 10-, 45-, and 70-kD dextrans (Invitrogen) were injected. Some experiments used DQ-OVA antigen (Invitrogen). Draining LNs were harvested at indicated times after injection. For in vitro antigen uptake studies, LNs or spleens were digested with collagenase D, and DCs were purified using $CD11c^+$ enrichment kits (Miltenyi Biotec). Isolated cells were next plated in cRPMI in 12- or 24-well plates with EαGFP along with CpG, where indicated, for 1 h at 37°C, washed twice with cRPMI, and incubated for an additional 2 h. DCs were washed and stained with indicated antibodies for flow cytometry. For TCR transgenic T cell immunization experiments, 1 d after adoptive transfer, recipient mice were immunized with OVA (Sigma-Aldrich) for OT-I and OT-II studies, or recombinant GP (MyBiosource, Inc.) for P14 and Smarta studies, with the draining LNs harvested 6 h (for image-based analysis) or 12 h (for flow cytometry) after immunization. In some experiments, OVA conjugated to APC was used. For DC-based immunization studies, enriched DCs were incubated with indicated quantities of OVA protein for 4 h and washed twice with PBS, and ∼30,000 pulsed DCs were injected in the footpads. 18–20 h later, animals were transferred with purified OT-I and OT-II T cells. For polyclonal immunization experiments, indicated quantities of GP or OVA protein along with CpG were injected in the footpads, with spleens isolated for analysis 7–8 d later. In some experiments, GP and CpG was injected in the ear pinnae, and some of the animals had the immunization site surgically removed 2 h after immunization. All animals in these exper-

iments were then treated with daily i.p. injections of 1 mg/kg FTY720 (Sigma-Aldrich) on days 2–5, and the draining LNs were harvested for analysis on day 6 post immunization.

Cell isolation and flow cytometry

For DC analysis, single-cell suspensions were prepared by treating isolated tissues with 400 U/ml collagenase D (Roche Applied Science) solution (1 part cRPMI:9 parts HBSS) for 25 min at 37°C with periodic agitation. EDTA (10 mM final concentration) was added to collagenase-digested cells for 1 min and then quenched with cold PBS. For T cell flow cytometry studies, homogenized tissues were not treated with collagenase D. Cells were stained with the indicated antibodies at 4°C for 30 min. For tetramer analysis, K^b:SIINFEKL tetramer conjugated to APC (NIH Tetramer Facility) was incubated with the cell suspension at 1:100 dilution for 1 h at room temperature before additional cell staining. Mouse V-β TCR screening panel was used for polyclonal response diversity measurements (BD Bioscience). For analysis of intracellular cytokine production, cells were first restimulated with 100 ng/ml phorbol 12-myristate 13-acetate, 1 µg/ml ionomycin (Sigma-Aldrich), and 1 µgl/ml monensin (Affymetrix) in cRPMI for 4 h at 37°C. Perm/Wash buffer (BD Biosciences) was used for intracellular cytokine staining. Cell suspensions were acquired on a LSR-II or LSRFortessa flow cytometer (BD Biosciences) and analyzed using FlowJo software (TreeStar).

Antibodies

The following antibodies were used for staining sections for imaging or isolated cells for flow cytometry: collagen-IV (rabbit polyclonal; Abcam), gp38 (clone 8.1.1; eBioscience), PNAd (clone Meca-79; BD Biosciences), ER-TR7 (clone sc-73355; Santa Cruz Biotechnology), CD11c (clone N418 or HL3; BioLegend), Lyve1 (clone Aly7; eBioscience), SIRPa (clone P84; BD Biosciences), CD11b (clone 5C6; AbD Serotec; clone M1/70; BioLegend), Y-Ae (clone eBioY-Ae; eBioscience), CD45.2 (clone 104; BioLegend), MHC II (clone M5/114.15.2; BioLegend), CD205 (clone NLDC-145; BioLegend), CD207 (clone 929F3.01; Dendritics), CD3 (clone 17A2; BioLegend), CD69 (clone H1.2F3; BioLegend), CD62L (clone Mel-14; BD Biosciences), CD8 (clone 53-6.7; BioLegend), IFNγ (clone XMG1.2; eBiosciences), CD127 (clone A7R34; BioLegend), and KLRG1 (clone 2F1; eBiosciences).

Confocal microscopy and whole 3D LN reconstruction

20-µm LN sections were prepared and imaged as previously described (Gerner et al., 2012). A Leica SP8 tiling confocal microscope equipped with a 40× 1.3-NA objective was used for the majority of confocal image acquisition, with the exception of DC/T cell cluster histo-cytometry studies, which used a 63× 1.4-NA objective. For whole LN reconstruction, depicted in the T cell cluster localization studies, fixed draining LNs were frozen in OCT compound (Tissue-Tek), sectioned into 150-µm slices using a cryostat, and serially imaged using a Zeiss-710 microscope. Chameleon-II 2P laser (Coherent) tuned to 800-nm wavelength and a 1.0-NA 20× water-immersion objective was used. Serial stack images were next recombined to reconstruct the whole 3D tissue in Imaris (Bitplane).

Two-photon intravital microscopy

Mice were anesthetized with isoflurane, and popliteal LNs were surgically exposed. Intravital imaging was performed using a previously published protocol (Bajénoff et al., 2006) using a Zeiss 710 tiling microscope equipped with a Chameleon laser and a 20× water immersion objective (NA 1.0; Zeiss). Raw imaging data were processed and analyzed with Imaris.

Histo-cytometry

Histo-cytometry analysis was performed as previously described, with some modifications (Gerner et al., 2012). In brief, multiparameter confocal images were first corrected for fluorophore spillover using the built-in Leica Channel Dye Separation module. For acquisition of single stained controls, UltraComp beads (Affymetrix) were incubated with fluorescently conjugated antibodies, mounted on slides, and imaged. Huygen's deconvolution (Scientific Volume Imaging) was applied only for analysis of DC subsets associated with T cell clusters. For other studies, deconvolution was not used. For analysis of antigen uptake by DCs, EαGFP signal was gated within $CD11c^+CD169^-Col.IV^-gp38^-$ voxels. For conduit association, antigen signal was gated within $Col.IV^+gp38^+Lyve1^-Meca79^-$ or $ER\text{-}TR7^+Lyve1^-CD11c^-$ structures. Voxel gating was performed using Imaris XT channel arithmetics module and Boolean expression algorithms. Conduit, LS, and DC surface objects were generated using the surface object creation wizard in Imaris, as detailed previously (Gerner et al., 2012), and their statistics were exported for further analysis into FlowJo software.

Histo-cytometry of DCs/T cell cluster contacts was performed as before (Gerner et al., 2015; Liu et al., 2015; Radtke et al., 2015). In brief, LNs were serially sectioned, and all regions with visible T cell clusters were imaged, with individual image files then recombined into a single composite image file representing all clusters per given LN. Clustered T cell signals were next identified by generating surface objects using a CD45.2 stain channel (transferred cells were $CD45.2^+$) and volumetric filtering in Imaris. All cluster objects were next separated into OT-I or OT-II clusters using mean channel intensity of OT-I and OT-II cells (transferred cells were labeled with fluorescent cell dyes), which were next used to mask the internal CD45.2 signal to generate dedicated, separated OT-I and OT-II cluster channels. Voxel gating for DC surface markers within $CD11c^+MHC\text{-}II^+B220^-CD3^-CD45.2^-$ voxels was performed using the Imaris XT channel arithmetics module and Boolean expression algorithms. DC surfaces were created via Imaris surface creation module, and the DC objects statistics were exported to Excel (Microsoft). Object statistics were combined into unified CSV files and finally

imported into FlowJo X software for cellular gating and analysis. For visual clarity, presented images were manipulated in Imaris and PowerPoint (Microsoft), with identical manipulation applied across experimental groups.

Statistical analysis

Statistical tests were selected based on appropriate assumptions with respect to data distribution and variance characteristics. No statistical methods were used to predetermine sample size. The statistical significance of differences in mean values was analyzed by a two-tailed unpaired Student's *t* test. Paired *t* test was performed only when comparing responses within the same experimental animal or tissue (indicated in the legend). ****, $P \leq 0.0001$; ***, $P \leq 0.001$; **, $P \leq 0.01$; and *, $P \leq 0.05$; NS, $P > 0.05$.

Online supplemental material

Fig. S1 shows conduit-dependent and -independent antigen dispersal in LNs. Fig. S2 demonstrates effects of DC positioning on antigen uptake and processing. Fig. S3 shows how DC positioning influences T cell clustering. Fig. S4 shows how antigen dose influences responses of TCR-transgenic T cells, and Fig. S5 examines this for polyclonal T cells. Video 1 shows antigen dispersal in LNs. Video 2 shows differential location $CD4^+$ versus $CD8^+$ T cell clustering.

ACKNOWLEDGMENTS

We thank members of the Lymphocyte Biology Section, Laboratory of Systems Biology, for many helpful comments during the course of these studies and for critical input during preparation of this manuscript. In particular, we acknowledge Drs. Rachel Gottschalk, Andrea Radtke, and Antonio Baptista for critical manuscript review.

This research was supported by the Intramural Research Program, National Institute of Allergy and Infectious Diseases, National Institutes of Health.

The authors declare no competing financial interests.

Author contributions: M.Y. Gerner designed, conducted, and analyzed experiments and wrote the manuscript; K.A. Casey and W. Kastenmuller contributed to experiment design and analysis; and R.N. Germain designed and interpreted experiments and helped write the manuscript.

Submitted: 21 February 2017

Revised: 16 June 2017

Accepted: 1 August 2017

REFERENCES

Allenspach, E.J., M.P. Lemos, P.M. Porrett, L.A. Turka, and T.M. Laufer. 2008. Migratory and lymphoid-resident dendritic cells cooperate to efficiently prime naive CD4 T cells. *Immunity.* 29:795–806. http://dx.doi.org/10.1016/j.immuni.2008.08.013

Alloatti, A., F. Kotsias, J.G. Magalhaes, and S. Amigorena. 2016. Dendritic cell maturation and cross-presentation: Timing matters! *Immunol. Rev.* 272:97–108. http://dx.doi.org/10.1111/imr.12432

Anandasabapathy, N., R. Feder, S. Mollah, S.W. Tse, M.P. Longhi, S. Mehandru, I. Matos, C. Cheong, D. Ruane, L. Brane, et al. 2014. Classical Flt3L-dependent dendritic cells control immunity to protein vaccine. *J. Exp. Med.* 211:1875–1891. http://dx.doi.org/10.1084/jem.20131397

Baekkevold, E.S., T. Yamanaka, R.T. Palframan, H.S. Carlsen, F.P. Reinholt, U.H. von Andrian, P. Brandtzaeg, and G. Haraldsen. 2001. The CCR7 ligand elc (CCL19) is transcytosed in high endothelial venules and mediates T cell recruitment. *J. Exp. Med.* 193:1105–1112. http://dx.doi.org/10.1084/jem.193.9.1105

Bajénoff, M., J.G. Egen, L.Y. Koo, J.P. Laugier, F. Brau, N. Glaichenhaus, and R.N. Germain. 2006. Stromal cell networks regulate lymphocyte entry, migration, and territoriality in lymph nodes. *Immunity.* 25:989–1001. http://dx.doi.org/10.1016/j.immuni.2006.10.011

Barnden, M.J., J. Allison, W.R. Heath, and F.R. Carbone. 1998. Defective TCR expression in transgenic mice constructed using cDNA-based alpha- and beta-chain genes under the control of heterologous regulatory elements. *Immunol. Cell Biol.* 76:34–40. http://dx.doi.org/10.1046/j.1440-1711.1998.00709.x

Buchholz, V.R., M. Flossdorf, I. Hensel, L. Kretschmer, B. Weissbrich, P. Gräf, A. Verschoor, M. Schiemann, T. Höfer, and D.H. Busch. 2013. Disparate individual fates compose robust CD8+ T cell immunity. *Science.* 340:630–635. http://dx.doi.org/10.1126/science.1235454

Calabro, S., A. Gallman, U. Gowthaman, D. Liu, P. Chen, J. Liu, J.K. Krishnaswamy, M.S. Nascimento, L. Xu, S.R. Patel, et al. 2016. Bridging channel dendritic cells induce immunity to transfused red blood cells. *J. Exp. Med.* 213:887–896. http://dx.doi.org/10.1084/jem.20151720

Celli, S., Z. Garcia, and P. Bousso. 2005. CD4 T cells integrate signals delivered during successive DC encounters in vivo. *J. Exp. Med.* 202:1271–1278. http://dx.doi.org/10.1084/jem.20051018

Cohn, L., and L. Delamarre. 2014. Dendritic cell-targeted vaccines. *Front. Immunol.* 5:255. http://dx.doi.org/10.3389/fimmu.2014.00255

Cyster, J.G. 2010. B cell follicles and antigen encounters of the third kind. *Nat. Immunol.* 11:989–996. http://dx.doi.org/10.1038/ni.1946

Dudziak, D., A.O. Kamphorst, G.F. Heidkamp, V.R. Buchholz, C. Trumpfheller, S. Yamazaki, C. Cheong, K. Liu, H.W. Lee, C.G. Park, et al. 2007. Differential antigen processing by dendritic cell subsets in vivo. *Science.* 315:107–111. http://dx.doi.org/10.1126/science.1136080

Eickhoff, S., A. Brewitz, M.Y. Gerner, F. Klauschen, K. Komander, H. Hemmi, N. Garbi, T. Kaisho, R.N. Germain, and W. Kastenmüller. 2015. Robust anti-viral immunity requires multiple distinct T cell-dendritic cell interactions. *Cell.* 162:1322–1337. http://dx.doi.org/10.1016/j.cell.2015.08.004

Gatto, D., K. Wood, I. Caminschi, D. Murphy-Durland, P. Schofield, D. Christ, G. Karupiah, and R. Brink. 2013. The chemotactic receptor EBI2 regulates the homeostasis, localization and immunological function of splenic dendritic cells. *Nat. Immunol.* 14:446–453. http://dx.doi.org/10.1038/ni.2555

Gerlach, C., J.C. Rohr, L. Perié, N. van Rooij, J.W. van Heijst, A. Velds, J. Urbanus, S.H. Naik, H. Jacobs, J.B. Beltman, et al. 2013. Heterogeneous differentiation patterns of individual CD8+ T cells. *Science.* 340:635–639. http://dx.doi.org/10.1126/science.1235487

Gerner, M.Y., W. Kastenmuller, I. Ifrim, J. Kabat, and R.N. Germain. 2012. Histo-cytometry: A method for highly multiplex quantitative tissue imaging analysis applied to dendritic cell subset microanatomy in lymph nodes. *Immunity.* 37:364–376. http://dx.doi.org/10.1016/j.immuni.2012.07.011

Gerner, M.Y., P. Torabi-Parizi, and R.N. Germain. 2015. Strategically localized dendritic cells promote rapid T cell responses to lymph-borne particulate antigens. *Immunity.* 42:172–185. http://dx.doi.org/10.1016/j.immuni.2014.12.024

Gerner, M.Y., P. Torabi-Parizi, and R.N. Germain. 2015. Strategically localized dendritic cells promote rapid T cell responses to lymph-borne particulate antigens. *Immunity.* 42:172–185. http://dx.doi.org/10.1016/j.immuni.2014.12.024

Gonzalez, S.F., V. Lukacs-Kornek, M.P. Kuligowski, L.A. Pitcher, S.E. Degn, Y.A. Kim, M.J. Cloninger, L. Martinez-Pomares, S. Gordon, S.J. Turley, and M.C. Carroll. 2010. Capture of influenza by medullary dendritic cells via SIGN-R1 is essential for humoral immunity in draining lymph nodes. *Nat. Immunol.* 11:427–434. http://dx.doi.org/10.1038/ni.1856

Gretz, J.E., A.O. Anderson, and S. Shaw. 1997. Cords, channels, corridors and conduits: Critical architectural elements facilitating cell interactions in the lymph node cortex. *Immunol. Rev.* 156:11–24. http://dx.doi.org/10.1111/j.1600-065X.1997.tb00955.x

Groom, J.R. 2015. Moving to the suburbs: T-cell positioning within lymph nodes during activation and memory. *Immunol. Cell Biol.* 93:330–336. http://dx.doi.org/10.1038/icb.2015.29

Guilliams, M., F. Ginhoux, C. Jakubzick, S.H. Naik, N. Onai, B.U. Schraml, E. Segura, R. Tussiwand, and S. Yona. 2014. Dendritic cells, monocytes and macrophages: A unified nomenclature based on ontogeny. *Nat. Rev. Immunol.* 14:571–578. http://dx.doi.org/10.1038/nri3712

Hansen, K.C., A. D'Alessandro, C.C. Clement, and L. Santambrogio. 2015. Lymph formation, composition and circulation: A proteomics perspective. *Int. Immunol.* 27:219–227. http://dx.doi.org/10.1093/intimm/dxv012

Heath, W.R., and F.R. Carbone. 2009. Dendritic cell subsets in primary and secondary T cell responses at body surfaces. *Nat. Immunol.* 10:1237–1244. http://dx.doi.org/10.1038/ni.1822

Hogquist, K.A., S.C. Jameson, W.R. Heath, J.L. Howard, M.J. Bevan, and F.R. Carbone. 1994. T cell receptor antagonist peptides induce positive selection. *Cell.* 76:17–27. http://dx.doi.org/10.1016/0092-8674(94)90169-4

Hor, J.L., P.G. Whitney, A. Zaid, A.G. Brooks, W.R. Heath, and S.N. Mueller. 2015. Spatiotemporally distinct interactions with dendritic cell subsets facilitates CD4+ and CD8+ T cell activation to localized viral infection. *Immunity.* 43:554–565. http://dx.doi.org/10.1016/j.immuni.2015.07.020

Hutchison, S., R.A. Benson, V.B. Gibson, A.H. Pollock, P. Garside, and J.M. Brewer. 2012. Antigen depot is not required for alum adjuvanticity. *FASEB J.* 26:1272–1279. http://dx.doi.org/10.1096/fj.11-184556

Irvine, D.J., M.A. Swartz, and G.L. Szeto. 2013. Engineering synthetic vaccines using cues from natural immunity. *Nat. Mater.* 12:978–990. http://dx.doi.org/10.1038/nmat3775

Itano, A.A., S.J. McSorley, R.L. Reinhardt, B.D. Ehst, E. Ingulli, A.Y. Rudensky, and M.K. Jenkins. 2003. Distinct dendritic cell populations sequentially present antigen to CD4 T cells and stimulate different aspects of cell-mediated immunity. *Immunity.* 19:47–57. http://dx.doi.org/10.1016/S1074-7613(03)00175-4

Jenkins, M.K., and J.J. Moon. 2012. The role of naive T cell precursor frequency and recruitment in dictating immune response magnitude. *J. Immunol.* 188:4135–4140. http://dx.doi.org/10.4049/jimmunol.1102661

Kamphorst, A.O., P. Guermonprez, D. Dudziak, and M.C. Nussenzweig. 2010. Route of antigen uptake differentially impacts presentation by dendritic cells and activated monocytes. *J. Immunol.* 185:3426–3435. http://dx.doi.org/10.4049/jimmunol.1001205

Kastenmüller, K., U. Wille-Reece, R.W. Lindsay, L.R. Trager, P.A. Darrah, B.J. Flynn, M.R. Becker, M.C. Udey, B.E. Clausen, B.Z. Igyarto, et al. 2011. Protective T cell immunity in mice following protein-TLR7/8 agonist-conjugate immunization requires aggregation, type I IFN, and multiple DC subsets. *J. Clin. Invest.* 121:1782–1796. http://dx.doi.org/10.1172/JCI45416

Kastenmüller, W., P. Torabi-Parizi, N. Subramanian, T. Lämmermann, and R.N. Germain. 2012. A spatially-organized multicellular innate immune response in lymph nodes limits systemic pathogen spread. *Cell.* 150:1235–1248. http://dx.doi.org/10.1016/j.cell.2012.07.021

Kastenmüller, W., K. Kastenmüller, C. Kurts, and R.A. Seder. 2014. Dendritic cell-targeted vaccines—Hope or hype? *Nat. Rev. Immunol.* 14:705–711. http://dx.doi.org/10.1038/nri3727

Katakai, T., T. Hara, J.H. Lee, H. Gonda, M. Sugai, and A. Shimizu. 2004. A novel reticular stromal structure in lymph node cortex: An immunoplatform for interactions among dendritic cells, T cells and B cells. *Int. Immunol.* 16:1133–1142. http://dx.doi.org/10.1093/intimm/dxh113

Kissenpfennig, A., S. Henri, B. Dubois, C. Laplace-Builhé, P. Perrin, N. Romani, C.H. Tripp, P. Douillard, L. Leserman, D. Kaiserlian, et al. 2005. Dynamics and function of Langerhans cells in vivo: Dermal dendritic cells colonize lymph node areas distinct from slower migrating Langerhans cells. *Immunity.* 22:643–654. http://dx.doi.org/10.1016/j.immuni.2005.04.004

Kitano, M., C. Yamazaki, A. Takumi, T. Ikeno, H. Hemmi, N. Takahashi, K. Shimizu, S.E. Fraser, K. Hoshino, T. Kaisho, and T. Okada. 2016. Imaging of the cross-presenting dendritic cell subsets in the skin-draining lymph node. *Proc. Natl. Acad. Sci. USA.* 113:1044–1049. http://dx.doi.org/10.1073/pnas.1513607113

Koup, R.A., and D.C. Douek. 2011. Vaccine design for CD8 T lymphocyte responses. *Cold Spring Harb. Perspect. Med.* 1:a007252. http://dx.doi.org/10.1101/cshperspect.a007252

Kurts, C., J.F. Miller, R.M. Subramaniam, F.R. Carbone, and W.R. Heath. 1998. Major histocompatibility complex class I-restricted cross-presentation is biased towards high dose antigens and those released during cellular destruction. *J. Exp. Med.* 188:409–414. http://dx.doi.org/10.1084/jem.188.2.409

Laidlaw, B.J., J.E. Craft, and S.M. Kaech. 2016. The multifaceted role of CD4(+) T cells in CD8(+) T cell memory. *Nat. Rev. Immunol.* 16:102–111. http://dx.doi.org/10.1038/nri.2015.10

Lämmermann, T., and M. Sixt. 2008. The microanatomy of T-cell responses. *Immunol. Rev.* 221:26–43. http://dx.doi.org/10.1111/j.1600-065X.2008.00592.x

Lee, H.K., M. Zamora, M.M. Linehan, N. Iijima, D. Gonzalez, A. Haberman, and A. Iwasaki. 2009. Differential roles of migratory and resident DCs in T cell priming after mucosal or skin HSV-1 infection. *J. Exp. Med.* 206:359–370. http://dx.doi.org/10.1084/jem.20080601

Lehmann, C.H., L. Heger, G.F. Heidkamp, A. Baranska, J.J. Lühr, A. Hoffmann, and D. Dudziak. 2016. Direct delivery of antigens to dendritic cells via antibodies specific for endocytic receptors as a promising strategy for future therapies. *Vaccines (Basel).* 4:8. http://dx.doi.org/10.3390/vaccines4020008

Li, M., G.M. Davey, R.M. Sutherland, C. Kurts, A.M. Lew, C. Hirst, F.R. Carbone, and W.R. Heath. 2001. Cell-associated ovalbumin is cross-presented much more efficiently than soluble ovalbumin in vivo. *J. Immunol.* 166:6099–6103. http://dx.doi.org/10.4049/jimmunol.166.10.6099

Lian, J., and A.D. Luster. 2015. Chemokine-guided cell positioning in the lymph node orchestrates the generation of adaptive immune responses. *Curr. Opin. Cell Biol.* 36:1–6. http://dx.doi.org/10.1016/j.ceb.2015.05.003

Lindquist, R.L., G. Shakhar, D. Dudziak, H. Wardemann, T. Eisenreich, M.L. Dustin, and M.C. Nussenzweig. 2004. Visualizing dendritic cell networks in vivo. *Nat. Immunol.* 5:1243–1250. http://dx.doi.org/10.1038/ni1139

Liu, H., K.D. Moynihan, Y. Zheng, G.L. Szeto, A.V. Li, B. Huang, D.S. Van Egeren, C. Park, and D.J. Irvine. 2014. Structure-based programming of lymph-node targeting in molecular vaccines. *Nature.* 507:519–522. http://dx.doi.org/10.1038/nature12978

Liu, Z., M.Y. Gerner, N. Van Panhuys, A.G. Levine, A.Y. Rudensky, and R.N. Germain. 2015. Immune homeostasis enforced by co-localized effector and regulatory T cells. *Nature.* 528:225–230. http://dx.doi.org/10.1038/nature16169

Lynn, G.M., R. Laga, P.A. Darrah, A.S. Ishizuka, A.J. Balaci, A.E. Dulcey, M. Pechar, R. Pola, M.Y. Gerner, A. Yamamoto, et al. 2015. In vivo characterization of the physicochemical properties of polymer-linked TLR agonists that enhance vaccine immunogenicity. *Nat. Biotechnol.* 33:1201–1210. http://dx.doi.org/10.1038/nbt.3371

Mandl, J.N., J.P. Monteiro, N. Vrisekoop, and R.N. Germain. 2013. T cell-positive selection uses self-ligand binding strength to optimize repertoire recognition of foreign antigens. *Immunity.* 38:263–274. http://dx.doi.org/10.1016/j.immuni.2012.09.011

Mempel, T.R., S.E. Henrickson, and U.H. Von Andrian. 2004. T-cell priming by dendritic cells in lymph nodes occurs in three distinct phases. *Nature.* 427:154–159. http://dx.doi.org/10.1038/nature02238

Merad, M., P. Sathe, J. Helft, J. Miller, and A. Mortha. 2013. The dendritic cell lineage: Ontogeny and function of dendritic cells and their subsets in the steady state and the inflamed setting. *Annu. Rev. Immunol.* 31:563–604. http://dx.doi.org/10.1146/annurev-immunol-020711-074950

Moyer, T.J., A.C. Zmolek, and D.J. Irvine. 2016. Beyond antigens and adjuvants: Formulating future vaccines. *J. Clin. Invest.* 126:799–808. http://dx.doi.org/10.1172/JCI81083

Murphy, T.L., G.E. Grajales-Reyes, X. Wu, R. Tussiwand, C.G. Briseño, A. Iwata, N.M. Kretzer, V. Durai, and K.M. Murphy. 2016. Transcriptional control of dendritic cell development. *Annu. Rev. Immunol.* 34:93–119. http://dx.doi.org/10.1146/annurev-immunol-032713-120204

Nikolich-Žugich, J., M.K. Slifka, and I. Messaoudi. 2004. The many important facets of T-cell repertoire diversity. *Nat. Rev. Immunol.* 4:123–132. http://dx.doi.org/10.1038/nri1292

Obst, R. 2015. The timing of T cell priming and cycling. *Front. Immunol.* 6:563. http://dx.doi.org/10.3389/fimmu.2015.00563

Obst, R., H.M. van Santen, D. Mathis, and C. Benoist. 2005. Antigen persistence is required throughout the expansion phase of a CD4(+) T cell response. *J. Exp. Med.* 201:1555–1565. http://dx.doi.org/10.1084/jem.20042521

Ohtani, O., Y. Ohtani, C.J. Carati, and B.J. Gannon. 2003. Fluid and cellular pathways of rat lymph nodes in relation to lymphatic labyrinths and Aquaporin-1 expression. *Arch Histol Cytol.* 66:261–72. http://dx.doi.org/10.1679/aohc.66.261

Oxenius, A., M.F. Bachmann, R.M. Zinkernagel, and H. Hengartner. 1998. Virus-specific major MHC class II-restricted TCR-transgenic mice: Effects on humoral and cellular immune responses after viral infection. *Eur. J. Immunol.* 28:390–400. http://dx.doi.org/10.1002/(SICI)1521-4141(199801)28:01<390::AID-IMMU390>3.0.CO;2-O

Palframan, R.T., S. Jung, G. Cheng, W. Weninger, Y. Luo, M. Dorf, D.R. Littman, B.J. Rollins, H. Zweerink, A. Rot, and U.H. von Andrian. 2001. Inflammatory chemokine transport and presentation in HEV: A remote control mechanism for monocyte recruitment to lymph nodes in inflamed tissues. *J. Exp. Med.* 194:1361–1374. http://dx.doi.org/10.1084/jem.194.9.1361

Pape, K.A., D.M. Catron, A.A. Itano, and M.K. Jenkins. 2007. The humoral immune response is initiated in lymph nodes by B cells that acquire soluble antigen directly in the follicles. *Immunity.* 26:491–502. http://dx.doi.org/10.1016/j.immuni.2007.02.011

Pennock, N.D., J.D. Kedl, and R.M. Kedl. 2016. T cell vaccinology: Beyond the reflection of infectious responses. *Trends Immunol.* 37:170–180. http://dx.doi.org/10.1016/j.it.2016.01.001

Pircher, H., K. Bürki, R. Lang, H. Hengartner, and R.M. Zinkernagel. 1989. Tolerance induction in double specific T-cell receptor transgenic mice varies with antigen. *Nature.* 342:559–561. http://dx.doi.org/10.1038/342559a0

Qi, H., W. Kastenmüller, and R.N. Germain. 2014. Spatiotemporal basis of innate and adaptive immunity in secondary lymphoid tissue. *Annu. Rev. Cell Dev. Biol.* 30:141–167. http://dx.doi.org/10.1146/annurev-cellbio-100913-013254

Radtke, A.J., W. Kastenmüller, D.A. Espinosa, M.Y. Gerner, S.W. Tse, P. Sinnis, R.N. Germain, F.P. Zavala, and I.A. Cockburn. 2015. Lymph-node resident CD8α+ dendritic cells capture antigens from migratory malaria sporozoites and induce CD8+ T cell responses. *PLoS Pathog.* 11:e1004637. http://dx.doi.org/10.1371/journal.ppat.1004637

Rantakari, P., K. Auvinen, N. Jäppinen, M. Kapraali, J. Valtonen, M. Karikoski, H. Gerke, I. Iftakhar-E-Khuda, J. Keuschnigg, E. Umemoto, et al. 2015. The endothelial protein PLVAP in lymphatics controls the entry of lymphocytes and antigens into lymph nodes. *Nat. Immunol.* 16:386–396. http://dx.doi.org/10.1038/ni.3101

Roozendaal, R., R.E. Mebius, and G. Kraal. 2008. The conduit system of the lymph node. *Int. Immunol.* 20:1483–1487. http://dx.doi.org/10.1093/intimm/dxn110

Roozendaal, R., T.R. Mempel, L.A. Pitcher, S.F. Gonzalez, A. Verschoor, R.E. Mebius, U.H. von Andrian, and M.C. Carroll. 2009. Conduits mediate transport of low-molecular-weight antigen to lymph node follicles. *Immunity.* 30:264–276. http://dx.doi.org/10.1016/j.immuni.2008.12.014

Savina, A., and S. Amigorena. 2007. Phagocytosis and antigen presentation in dendritic cells. *Immunol. Rev.* 219:143–156. http://dx.doi.org/10.1111/j.1600-065X.2007.00552.x

Schnorrer, P., G.M. Behrens, N.S. Wilson, J.L. Pooley, C.M. Smith, D. El-Sukkari, G. Davey, F. Kupresanin, M. Li, E. Maraskovsky, et al. 2006. The dominant role of CD8+ dendritic cells in cross-presentation is not dictated by antigen capture. *Proc. Natl. Acad. Sci. USA.* 103:10729–10734. http://dx.doi.org/10.1073/pnas.0601956103

Sixt, M., N. Kanazawa, M. Selg, T. Samson, G. Roos, D.P. Reinhardt, R. Pabst, M.B. Lutz, and L. Sorokin. 2005. The conduit system transports soluble antigens from the afferent lymph to resident dendritic cells in the T cell area of the lymph node. *Immunity.* 22:19–29. http://dx.doi.org/10.1016/j.immuni.2004.11.013

Steinman, R.M., M. Pack, and K. Inaba. 1997. Dendritic cells in the T-cell areas of lymphoid organs. *Immunol. Rev.* 156:25–37. http://dx.doi.org/10.1111/j.1600-065X.1997.tb00956.x

Stone, J.D., A.S. Chervin, and D.M. Kranz. 2009. T-cell receptor binding affinities and kinetics: Impact on T-cell activity and specificity. *Immunology.* 126:165–176. http://dx.doi.org/10.1111/j.1365-2567.2008.03015.x

Surh, C.D., and J. Sprent. 2008. Homeostasis of naive and memory T cells. *Immunity.* 29:848–862. http://dx.doi.org/10.1016/j.immuni.2008.11.002

Tacken, P.J., I.J. de Vries, R. Torensma, and C.G. Figdor. 2007. Dendritic-cell immunotherapy: From ex vivo loading to in vivo targeting. *Nat. Rev. Immunol.* 7:790–802. http://dx.doi.org/10.1038/nri2173

Tscharke, D.C., N.P. Croft, P.C. Doherty, and N.L. La Gruta. 2015. Sizing up the key determinants of the CD8(+) T cell response. *Nat. Rev. Immunol.* 15:705–716. http://dx.doi.org/10.1038/nri3905

van der Burg, S.H., R. Arens, F. Ossendorp, T. van Hall, and C.J. Melief. 2016. Vaccines for established cancer: Overcoming the challenges posed by immune evasion. *Nat. Rev. Cancer.* 16:219–233. http://dx.doi.org/10.1038/nrc.2016.16

Woodruff, M.C., B.A. Heesters, C.N. Herndon, J.R. Groom, P.G. Thomas, A.D. Luster, S.J. Turley, and M.C. Carroll. 2014. Trans-nodal migration of resident dendritic cells into medullary interfollicular regions initiates immunity to influenza vaccine. *J. Exp. Med.* 211:1611–1621. http://dx.doi.org/10.1084/jem.20132327

Yi, T., and J.G. Cyster. 2013. EBI2-mediated bridging channel positioning supports splenic dendritic cell homeostasis and particulate antigen capture. *eLife.* 2:e00757. http://dx.doi.org/10.7554/eLife.00757